ISSN 0915-6348

NATIONAL INSTITUTE FOR FUSION SCIENCE

Studies on Wave Analysis and Electric Field in Plasmas

H. Sanuki

(Received - June 27, 1997)

NIFS-PROC-33 July 1997

RESEARCH REPORT
NIFS-PROC Series

This report was prepared as a preprint of work performed as a collaboration research of the National Institute for Fusion Science (NIFS) of Japan. This document is intended for information only and for future publication in a journal after some rearrangements of its contents.

Inquiries about copyright and reproduction should be addressed to the Research Information Center, National Institute for Fusion Science, Nagoya 464-01, Japan.

NAGOYA, JAPAN

Studies on Wave Analysis and Electric Field in Plasmas

Heiji Sanuki

National Institute for Fusion Science
Nagoya, 464-01, Japan

Abstract

Some aspect of the theoretical and experimental activities in the problems associated with radial electric field in toroidal plasmas are surveyed. The present lecture consists of the two parts. The first part is oriented to the brief review of the stability theories to analyze the micro-instabilities in an inhomogeneious plasma ,and also to the effect of radial electric field on these instabilities and fluctuation -induced anomalous transport. The second part overviews the theoretical models to determine selfconsistently the radial electric field and the loss fluxes in toroidal plasmas ,and the cooperative mechanism among the electric field, loss of energetic particles, anomalous transport(bipolar) and confinement characteristics is also discussed. Experimental observations and related theories on plasma rotations in both past and existing toroidal devices such as tokamaks, stellarators and heliotron/torsatron are revisited and also are briefly reviewed. Comparison is made between theoretical predictions and experimental observations particularly in the NBI and ECH plasmas of the Compact Helical System(CHS) and the Wendelstein VII-A(WVII-A) devices.

This article was prepared for the lecture at "Frontier of Physics in Fusion Relevant Plasmas", 1996 Asian Science Seminar, 20-29 October 1996, Hefei- Tunxi , Anhui Province, P. R. China.

keywords: radial electric field, stability analyses, neoclassical and anomalous transports, plasma rotation, tokamak and helical systems

Contents

1. Introduction

Radial electric field has been experimentally observed in toroidal plasma confinement devices such as tokamaks[1-4] , stellarators[5] and heliotron/torsatrons[6,7]. These experimental observations may provide the database for an understanding of the physics associated with radial electric field, i.e.,the electric field is believed to play important roles in the suppression and/or enhancement of various types of microinstabilities[8-11], the neoclassical[12,13] and anomalous[14,15] plasma transports, and consequential confinement improvement such as H-mode[16-18]. Although a large number of database for the effect of radial electric field has been accumulated experimentally and theoretically, the physics involved has not been completely understood, and there are still fundamental questions such as, whether the electric field always be a useful tool, i. e., if the spontaneous electric field in plasma is sufficient or if any specific idea to control the electric field is required. To reply these questions, the cooperative mechanism among electric field and physical processes involved , namely, loss of energetic particles, neoclassical and anomalous transports, heating and so on should be clarified[19,20]. The mutual relation involved in these physical processes is roughly sketched in Fig.1.

Various theoretical models related to the electric field generation process and its influence on the stability and transport have been proposed[21-25]. On the other hand, much attention has been paid on how to control the electric field and consequently the confinement improvement. Several approaches to the active control of electric field have been discussed, by adjusting the ion and/or electron loss channels due to the selective NBI and/or ECH heating, biasing and so on. For the complete comparison between theoretical predictions and experimental observations , the high-time- and spatial- resolved measurement of plasma parameters are required. Recent considerable progress on the measurement techniques such as the charge exchange recombination spectroscopy(CXS)[26,27],heavy ion beam probing(HIBP)[28,29], and laser blow-off Lithium beam probing[30], may realize the detailed analysis of radial electric field profile and confinement characteristics in the whole plasma region.

In this lecture, we overview some aspect of the theoretical and experimental studies of the electric field generation process and it's influence on the stability and transport. In the next section, we briefly survey the wave analyses for linear plasma waves on the basis of the fluid and kinetic description. Particularly, the WKB analysis based on both the second order differential equation and the integral equation in wave number space(k-space) are discussed. This analytical method is applied to study the effect of electric field on the typical microinstsbilities such as drift waves in this section. In Section 3, the reduction of anomalous transport due to the sheared rotation(gradient of electric field) will be briefly discussed. Theoretical modeling on the electric field generation in toroidal plasmas is presented in Sec.4. In Section 5, both past and recent

year's plasma rotation studies are also discussed theoretically and experimentally. Current experimental results on the electric field structure in helical devices such as CHS and WVII-A are briefly introduced, and comparison between theoretical predictions and experimental observations will be made in Sec.6. The last section will be devoted to the summary.

2. Brief Survey of Stability Analysis for Linear Plasma Waves

2-1. Key features characterizing plasma waves

We here summarize typical analytical methods for linear plasma waves. It should be noted that these plasma waves are characterized by the following features :

* Modes : electron modes or ion modes, electrostatic or electromagnetic,
* Direction of propagation : parallel or perpendicular to the magnetic field,
* Collisionality : collisional or collisionless,
* Velocity distribution : Maxwellian or non- Maxwellian,
* Uniformity : uniform or nonuniform magnetic field, namely magnetic shear or no shear,
* Inhomogeneity : homogeneous or inhomogeneous density, temperature, both density and temperature , electric field,
* Particle trapping : trapped or untrapped,
* Boundary : bounded or unbounded,
* Localization : local or nonlocal,
* Evolution characteristics : temporal or spatial,
* Nonlinearity : linear or nonlinear.

2-2. Derivation of wave equation for low frequency modes (fluid description)

Noting that the vector $\vec{B}$ can be expressed by the rotation of vector $\vec{A}$ as

$$\vec{B} = \nabla \times \vec{A} \ , \tag{1}$$

and the electric field $\vec{E}$ can be expressed by a scalar potential φ and $\vec{A}$ as

$$\vec{E} = -\nabla \varphi - \frac{1}{c}\frac{\partial \vec{A}}{\partial t} \ . \tag{2}$$

Maxwell equations reduce to the following wave equations

$$\nabla^2\varphi - \frac{1}{c^2}\frac{\partial^2\varphi}{\partial t^2} = -4\pi\rho, \tag{3}$$

$$\nabla^2\vec{A} - \frac{1}{c^2}\frac{\partial^2\vec{A}}{\partial t^2} = -\frac{4\pi}{c}\vec{J}, \tag{4}$$

where ρ and $\vec{J}$ are the charge and current densities, respectively and we imposed the supplementary condition

$$\nabla\cdot\vec{A} + \frac{1}{c}\frac{\partial\varphi}{\partial t} = 0. \tag{5}$$

From the parallel and perpendicular components of these equations (3)-(5), we obtain the coupled equations for φ , $\vec{A}_\perp$ and $A_{//}$,

$$\nabla\cdot\vec{A} + \frac{1}{c}\frac{\partial\varphi}{\partial t} = 0, \tag{5}$$

$$\nabla_{//}(\Delta A_{//} - \frac{1}{c^2}\frac{\partial^2 A_{//}}{\partial t^2}) = \frac{4\pi}{c}\nabla_\perp\cdot\sum_{j=e,i} n_j q_j \vec{V}_{\perp j}, \tag{6}$$

$$(\Delta\vec{A}_\perp - \frac{1}{c^2}\frac{\partial^2\vec{A}_\perp}{\partial t^2}) = -\frac{4\pi}{c}\sum_j n_j q_j \vec{V}_{\perp j}. \tag{7}$$

We are now in the position to determine $\vec{A}_\perp$ in eqs.(5)-(7) and assume the qusineutrality condition and so called drift approximation. From the fluid equation of motion

$$m_j n_j[\frac{\partial\vec{V}_j}{\partial t} + (\vec{V}_j\cdot\nabla)\vec{V}_j = q_j n_j(\vec{E} + \frac{1}{c}\vec{V}_j\times\vec{B}) - \nabla p - \nabla\cdot\vec{\pi} + m_j n_j\vec{g}_j, \tag{8}$$

we obtain by taking the vector product of eq.(8) with $\hat{z}$ (here assume that $B = B_0\hat{z}$)

$$\vec{V}_{\perp j} = \frac{c}{B_0}\hat{z}\times(\nabla_\perp\varphi + \frac{1}{c}\frac{\partial\vec{A}_\perp}{\partial t}) \quad (V_E:\ E\times B \text{ drift})$$

$$+\frac{c}{B_0}\frac{m_j}{q_j}\hat{z}\times\frac{d\vec{V}_{\perp j}}{dt} \qquad (V_{pj}:\ \text{polarization drift})$$

$$+\frac{c}{q_j n_j B_0}\hat{z}\times\nabla p \qquad (V_{Dj}:\ \text{diamagnetic drift}) \qquad (9)$$

$$-\frac{m_j c}{q_j B_0}\hat{z}\times\vec{g}_j \qquad (V_{gj}:\ \text{gravitational drift})$$

$$+\frac{c\hat{z}\times\nabla\cdot\vec{\vec{\pi}}}{q_j n_j B_0} \qquad (V_\pi:\ \text{drift due to stress tensor})$$

In eq.(9), we note that $V_{pj} << V_E$, which is valid under the frequency ordering $\omega << \omega_{cj}$,where ω_{cj} is the cyclotron frequency for j-species.

Let us consider the contribution of $\vec{A}_\perp$ and $E_{//}$ components. Substituting eq.(9) into eq.(7) and noting that E×B drift term (V_E) does not contribute totally to the net current because V_E is charge independent, we have

$$[k^2 - \frac{\omega^2}{c^2} - \frac{\omega(\omega - k_\perp v_{Di})}{V_A^{\,2}}]A_\perp \cong -\frac{c^2}{V_A^{\,2}}\frac{k_\perp}{c}(\omega - k_\perp v_{Di})\varphi \ , \qquad (10)$$

We here dropped the contribution from the electron polarization since $m_e/m_i << 1$.. If $\omega^2/c^2 \to 0$ in eq.(10), the left hand side(lhs) of eq.(10) gives the dispersion relation of the compressional Alfven wave , which couples to the shear Alfven wave in the right hand side(rhs) of eq.(10). When one consider the dispersion branch of the shear Alfven wave, equation(10) yields the relation

$$(\frac{\omega}{c}A_\perp)/(k_\perp\varphi) = \frac{k_{//}^{\,2}}{k_\perp^{\,2}} \ , \qquad (11)$$

where we used the notations, $k_{//} = 2\pi/L_{//}$ and $k_{\perp} = 2\pi/L_{\perp}$. Therefore, $A_{\perp}$ - component can be neglected provided that

$$(\frac{L_{\perp}}{L_{//}})^2 << 1. \tag{12}$$

This approximation is called as the "long thin approximation", which is often used in the tandem mirror configuration. But , this approximation breaks down in the mirrors with large mirror ratio ($L_{//} \approx L_{\perp}$). If we evaluate $E_{//}$ -component in the shear Alfven dispersion branch, we have

$$\frac{E_{//}}{E_{\perp}} = -i\frac{k_{//}\varphi - \omega/c A_{//}}{E_{\perp}} \approx \frac{k_{//}\varphi}{k_{\perp}\varphi}\frac{\omega^2}{k_{//}^2 c^2} << 1. \tag{13}$$

So, $E_{//}$ is negligibly small for this mode. We next consider the coupled equations among φ , $A_{\perp}$ and $A_{//}$. To do so, we introduce the so called the Kadomtsev notation, $\hat{E}_{\perp} = -\nabla_{\perp}\varphi$ and $\hat{E}_{//} = -\nabla_{//}\psi$. We finally obtain the following relations

$$\psi = k_{\perp}^2 \rho_i^2 \frac{V_A^2 k_{//}^2}{\omega(\omega_{*e} - \omega) + k_{\perp}^2 \rho_i^2 V_A^2 k_{//}^2}\varphi \ , \tag{14a}$$

$$\psi = \varphi - \frac{\omega}{k_{//}c} A_{//} , \tag{14b}$$

$$(\omega^2 + \omega\omega_{*i})\phi - V_A^2 k_{//}^2 (\omega/k_{//}c) A_{//} = 0 , \tag{15}$$

which give the dispersion relation[31]

$$\omega(\omega_{*e} - \omega)[\omega^2 + \omega_{*i}\omega - k_{//}^2 V_A^2] + \omega(\omega + \omega_{*i})k_{\perp}^2 \rho_i^2 k_{//}^2 V_A^2 \approx 0, \tag{16}$$

which describes the coupling between acoustic mode and shear Alfven mode due to the finite Larmor radial effect and this relation has been extended through including a gravitational force[32].

2-3. WKB analysis based on kinetic description

There are various wave phenomena in plasmas such as propagation, absorption, mode-conversion, mode- coupling and so on. Kinetic approach based on Maxwell-Vlasov equations is required to study these topics. Typical analytical methods to study the plasma waves are summarized as

(a) Local dispersion relation,

(b) Eigenvalue program based on second order differential equation ,

(c) Eigenvalue problem based on integral equation .

It should be noted that we apply a convenient method among these analyses , depending on what kind of information we want. As for the method to solve the differential and integral equations is concerned, we have powerful tools such as the WKB(Wenzel- Krammers- Brillouin) method and the direct numerical analyses based on such as the shooting method for differential equation and the base function expansion method for integral equation. Analytical technique sensitively depends on the situation whether the mode is electrostatic or electromagnetic, the mode number is low or high , and also the instability is weak or strong. We hereafter restrict our discussions to the WKB analysis in this lecture. We note that the WKB analytical method for the electrostatic waves have been well developed for both differential and integral equations, particularly in case of weak unstable modes.

2-3-1. WKB solution of second order differential equation

For simplicity, let us consider electrostatic modes in an inhomogeneious plasma,where the inhomogeneity is assumed to be along x-direction. If we represent the potential profile as

$$\phi(\bar{r},t) = \phi_0 \exp[i(\int k_x(x')dx' + k_y y + k_z z - \omega t)] , \tag{17}$$

then, we obtain the local dispersion relation

$$\varepsilon[k_x(x), k_y, k_z : \omega]\phi = 0 , \tag{18}$$

which yields $\omega = \omega(k_x(x), k_y, k_z)$. We get the qualitative information, but not quantitative one because it is hardly to determine the wave profile and dispersion relation consistently.

Next , we are going to the eigenvalue problem on the basis of the second order differential equation. If we replace the x-component of wave number, $k_x(x)$ as

$$k_x \rightarrow -i\frac{\partial}{\partial x} + k_{x0} \ , \tag{19}$$

and expand the modified Bessel function term and keep up to the second order with respect to $k_x\rho$ ($k_x\rho << 1$) ,

$$I_0 e^{-b} \approx 1 - b \ = 1 - \rho^2[k_y^{\ 2} - \frac{\partial^2}{\partial x^2}] \quad , \quad b = \rho^2 k_\perp^{\ 2} = \rho^2(k_x^{\ 2} + k_y^{\ 2}) \ , \tag{20}$$

we finally get

$$\frac{d^2}{dx^2}\phi - Q(x)\phi = 0 \ , \tag{21}$$

which can be regarded as an eigenvalue problem and cases with $k_x\rho \geq 1$ will be discussed later. The WKB solution based on eq.(21) has been discussed by many authors[33]. We here briefly explain the WKB solution. If Q(x) is a real and slowly- varying function of x, equation(21) can be solved by the WKB method when $\phi \rightarrow 0$ as $x \rightarrow \pm\infty$. The solution is given as

$$\phi(x) \cong Q^{-1/4}(x)\exp[\pm\int_{x_1}^{x}\sqrt{Q(x')}dx'] \ , \tag{22}$$

and " quantization condition " or dispersion relation is also represented by

$$\int_{x_1}^{x_2}[-Q(x)]^{1/2}dx = \pi(n + 1/2) \ , \quad (n = 0,1,\cdots) \ . \tag{23}$$

In general, however, Q(z) is complex and we define two turning points of Q(z) in the complex plane , z_1 and z_2, where $Q(z_1) = Q(z_2) = 0$. If one define a curve C as $Q(z_c = x_c + iy_c)$ is real along C, then $Q(z_c) < 0$ $(z_1 < z_c < z_2)$ and $Q(z_c) > 0$ $(z_c < z_1, z_c > z_2)$, and we obtain along C

$$\frac{d^2\phi(z_c)}{dz_c^{\ 2}} - Q(z_c)\phi(z_c) = 0 \ . \tag{24}$$

Following the same way as eq.(21), equation (24) gives the WKB solution

$$\phi(z_c) = \sum_{+,-} A_{\pm} Q^{-1/4}(z_c) \exp[\pm \int_{z_1, z_2}^{z_c} Q^{1/2}(z)\, dz] \ , \tag{25}$$

and an eigenvalue relation can be easily obtained from the connection formulae

$$\int_{z_1}^{z_2} [-Q(z_c)]^{1/2} dz_c = \pi(n + 1/2), \ \ (n = 0,1,\cdots) . \tag{26}$$

An example on the curve C in z-plane and corresponding eigenfunction are roughly illustrated in Fig.2.

2-3-2. Eigenmode analysis(WKB method) based on integral equation in k- space

We first note that this analysis is applicable to the highly localized modes in case of $k_x \rho \geq 1$, where eigenvalue problem based on eq.(21) or eq.(24) breaks down. If one defines the potential form as

$$\phi(\vec{r}, t) = \int_{-\infty}^{+\infty} dk \exp[i(kx + k_y y + k_z z - \omega t)] \ , \tag{27}$$

we have the following integral equation in k-space

$$(k^2 + k_y^{\ 2} + k_z^{\ 2})\phi(k) = \int K(k', k : \omega)\phi(k')dk' \ , \tag{28}$$

where in the limit of $k' \rightarrow k$, equation(28) yields the dispersion relation for electrostatic modes in a homogeneous plasma. We are now in the position how to solve the integral equation(28). There are two methods, namely ,WKB type technique and numerical analysis. Hereafter, we restrict our discussions to the WKB analysis based on the integral equation in k-space.

Let us introduce the eikonal function in both configuration and wave number spaces,which are convenient to study the WKB solution. If kL>>1, where k is the wave number and L is the

characteristic scale length, the eikonal function in real space is represented by

$$\phi(x) = \exp[-i\int^{x} f(x')dx'] , \tag{29}$$

and the eikonal function in k-space is also defined as

$$\phi(k) = \exp[-i\int^{k} g(k')dk'] . \tag{30}$$

Using $(kL)^{-1}$ expansion, we can determine f(x) or g(k) by solving the equation after substitution of eq.(29) or eq.(30) into the integral equation[8,34]. We next consider the physical meaning of the eikonal function g(k). Using eq.(30), the potential form is given as

$$\phi(x) = \int dk \exp[-i\int_{k_0}^{k} g(k')dk' + ikx] . \tag{31}$$

Then, we carry out the integration in eq.(30) by the steepest decent method and we have

$$\phi(\mathrm{x}) \cong \sqrt{-2\pi i / g(k_s)}\exp[-i\int_{k_0}^{k_s} g(k')dk' + ik_s x] , \tag{32}$$

where k_s corresponds to the wave number at the saddle point of the integration, which is given by $x = g(k_s)$. Therefore, eikonal function in k-space g(k) represents the x- coordinate with local wavenumber k_s. Substitution of $\phi(k)$ into the integral equation (28) yields

$$F(k) = \int_{-\infty}^{\infty} dk' K(k,k')\exp[-i\int_{k}^{k'} g(k'')dk''], \tag{33}$$

where $F(k) = k^2 + k_y^2 + k_z^2$ and we used the simplified notation $K(k', k;\omega) = K(k', k)$, and this equation is similar to the three wave coupling equation, where the wavenumber matching condition, $k = k' + \kappa$. Here, we note that $\kappa \approx L^{-1}$ and $|k - k'| \le L^{-1}$ even for kL>>1.

We next consider the derivation of the " quantization condition " based on eq.(30). To do so, we use the following asymptotic expansion of eikonal function

$$g(k) = g_0(k) + g_1(k) + \cdots \ , \tag{34}$$

$$g(k^{''}) \cong g(k) + (k^{''} - k)dg/dk + (higher\ order). \tag{35}$$

It should be noted that the first and the second terms in eqs.(34) and (45) are $O(L)$ and $O(L \cdot \gamma_{Lk})$, respectively. From each order with respect to the $(kL)^{-1}$ expansion, namely, $O(L)$ and $O(L \cdot \gamma_{Lk})$, we have

$$0 = H(k, g_0; \omega) \equiv \int K(k,k^{'}) \exp[-i(k^{'} - k)g_0(k)]dk^{'} - F(k) \ , \tag{36}$$

$$g_1(k) = -\left(\partial^2 H/\partial g_0^{\ 2}\right)\left(\partial H/\partial g_0\right)^{-1} dg_0/dk \ . \tag{37}$$

From eq.(36), we obtain the relation between g_0 and k for fixed ω. In general, the curve g= $g(k)$ for localized modes becomes a closed loop in (k,g) plane, which is shown in Fig.3. Here, x_{t1} and x_{t2} are the turning points in x coordinate and also k_{t1} and k_{t2} are the turning points in k space. In this situation, localized mode can be constructed by the superposition of two independent plane waves with k, the range of which is given as $k_{t1} < k < k_{t2}$. From the connection formula between the solutions inside and outside of the turning points, we have the relation

$$\oint (g_0 + g_1)dk = 2(n+1)\pi \ , \tag{38}$$

which gives after substitution of eq.(37) and carrying out the integration

$$\oint g_0(k)dk = 2(n + 1/2)\pi \ . \tag{39}$$

This relation is so called " quantization condition " , in other words, this corresponds to the dispersion relation in plasma physics . It should be noted that the asymptotic wave profile near turning point (k_t , g_t) can be represented approximately by the Airy function as a WKB solution.

2-3-3. New nonlocal analysis

We here consider the nonlocal analysis of Vlasov plasma in a weakly dissipative case on the basis of the WKB method mentioned in Sec. 2-3-2. When the dissipative effect is weak, namely, $\omega_r >> \omega_i$, where ω_r and ω_i are the real and imaginary parts of frequency, respectively, the imaginary part H_1 of $H[k, g_0(k);\omega]$ is small compared with the real part H_0 . In this case , we can expand eq.(36) as

$$0 \cong H_0(k, g_{0r};\omega_r) + [iH_1(k, g_{0r};\omega_r) + i\omega_i \frac{\partial H_0}{\partial \omega_r} + g_{0i} \frac{\partial H_0}{\partial g_{0r}}] \ , \tag{40}$$

where we put $g_0 = g_{0r} + g_{0i}$ and $\omega = \omega_r + i\omega_i$ and used the relations $H_0 >> H_1$ and $\omega_r >> \omega_i$. The real and imaginary parts of " quantization condition " give the following relations

$$H_0(k, g_{0r};\omega_r) = 0 \ , \tag{41}$$

$$g_{0i} = -i\left(\frac{\partial H_0}{\partial g_{0r}}\right)^{-1} (\omega_i \frac{\partial H_0}{\partial \omega_r} + H_1) \ . \tag{42}$$

Equation(41) can be regarded as the Hamiltonian system, which is solved by " orbit integration " and we obtain

$$\frac{dk}{dt} = (\frac{\partial H_0}{\partial g_{0r}}) \Big/ (\frac{\partial H_0}{\partial \omega_r}) \ , \tag{43}$$

$$\frac{dg_{0r}}{dt} = -(\frac{\partial H_0}{\partial k}) \Big/ (\frac{\partial H_0}{\partial \omega_r}) \ , \tag{44}$$

provided that the initial values of k and g_{0r} satisfy the relation, $H_0[k(t=0), g_{0r}(t=0);\omega_r] = 0$. The zeroth order of the quantization condition (39) reduces to

$$\oint g_{0r} \frac{dk}{dt} dt = 2(n + \tfrac{1}{2})\pi \ , \tag{45}$$

which determines the real frequency ω_r . From the first order of eq.(39), the growth rate is obtained by

$$\omega_i = -\oint\left[H_1\Big/\left(\frac{\partial H_0}{\partial g_{0r}}\right)\right]dk\left\{\oint\left(\frac{\partial H_0}{\partial \omega_r}\Big/\frac{\partial H_0}{\partial g_{0r}}\right)dk\right\}^{-1} . \qquad (46)$$

To demonstrate the usefulness of the eigenmode analysis mentioned above, we apply this method to electrostatic drift waves. It is plausible that important waves in an inhomogeneous plasma are drift waves. Without magnetic shear effect, drift waves may be localized in the following cases: (1)the drift frequency has a peak at a critical position of plasma density, $\partial\omega_*/\partial x = 0$ and (2) the drift frequency does not have a peak, $\partial\omega_*/\partial x \neq 0$ for all x, but the quasi-neutrality condition is not imposed because this condition is invalid at the periphery of plasma. In this lecture, we restrict our discussions to the case (2). Let us consider a drift wave in a Gaussian density distribution, $n_0(x) = N_0\exp(-x^2/2\lambda^2)$,where λ is the scale length of density inhomogeneity and we assume $\rho/\lambda << 1$. Since the drift frequency increases with x for this density profile, we can apply the quasi-neutrality condition in order for modes to localize in the real space. In the following discussions, for simplicity, the finite Larmor radius effect for ions is taken into account and the frequency ordering for drift waves, $v_i << \omega/k_{//} << v_e$ is applied. Under these conditions, eq.(41) is approximately given as

$$H_0[k, g_{0r}(k);\omega] = (\tilde{k}^2 + \tilde{k}_\perp^{\,2} + \tilde{k}_{//}^{\,2}) + \frac{\omega_{pi}^{\,2}}{\omega_{ci}^{\,2}}\exp\left(-\frac{\tilde{g}_0^{\,2}}{2}\right)$$

$$\times\left(1 + \frac{T_i}{T_e} - I_0(b)\exp(-b) - \frac{\omega_{*i}}{\omega}\tilde{g}_0 I_0(b)\exp(-b)\right), \qquad (47)$$

where $\tilde{k}^2 = k^2\rho_i^{\,2}$, $\tilde{k}_\perp^{\,2} = k_\perp^{\,2}\rho_i^{\,2}$, $\tilde{k}_{//}^{\,2} = k_{//}^{\,2}\rho_i^{\,2}$, $\omega_{pi}^{\,2} = 4\pi N_0 e^2/M_i$, $\tilde{g}_0 = g_{0r}/\lambda$, $b = \tilde{k}^2 + \tilde{k}_\perp^{\,2}$ and $\omega_{*i} = (cT_i/eB)(k_\perp/\lambda)$. Here, we abbreviated the explicit form of H_1. We numerically solve eqs.(43) and (44) for given relation (47) and determine the eigenfrequency and the growth rate from eqs.(45) and (46). The results for $\tilde{g}_0$ (k) for given values of ω_r/ω_{*i} corresponding to given radial mode number are represented in Figs.(4a)-(4c).

Let us explain briefly the physical picture of these figures. Several contour lines express the constant ω_r/ω_{*i} surfaces and $(\tilde{g}_{0t}, \tilde{k}_t)$ be the turning point and $\tilde{g}_{oc}$ be the center of the contours. As mentioned before, the corresponding mode is purely oscillatory between $-\tilde{k}_t$ and $\tilde{k}_t$, and must be exponentially increasing or decreasing as one moves away from one to the other when crossing turning points. Also, we can determine the localization center ($\tilde{g}_{oc}$ means the position of the center of localized modes), the localization region and the corresponding wavenumber. The wave structure becomes more symmetric around the localization center and the wavenumber also increases as $k_\perp \rho_i$ becomes large. The results for ω_r/ω_{*i} and ω_i/ω_{*i} vs. $k_\perp \rho_i$ for a cesium plasma are illustrated in Fig.5.

Analyses based on the WKB method in k-space were extended into more general cases such as multi-species plasma including energetic electron component in bumpy tori [9], electromagnetic modes[35,36], drift wave[37] in clyndrical plasma and DCLC[38] in slab geometry. Also,the derivation of integral equation in k-space and numerical method to solve this integral equation has been discussed in clyndrical geometry . This numerical technique was applied to drift waves, DC modes[39] and DCLC modes[40]. We explain some debatable topics on WKB analysis. Integral equation for electromagnetic modes is given in a general form

$$\int_{-\infty}^{\infty} \vec{\mathrm{K}}(\mathrm{k},\mathrm{k}') \cdot \vec{E}(k')dk' = 0 , \tag{48}$$

where $\vec{K}$ is the 3×3 metrix tensor and $\vec{E}$ is the field vector. The quantization condition in the vector system has been discussed by Berk and Pfirsh[41] and Watanabe et al.[36]. Berk and Pfiirsh discussed the theoretical derivation of quantization condition

$$\oint [k(x) + \delta k(x)]dk = (2n+1)\pi \quad , n = 0,1,2\cdots \tag{49}$$

where $\delta k(x)$ is the electromagnetic correction and $\delta k(x) \to 0$ in case of electrostatic, and we have well-known relation. Also, Watanabe et al. studied the numerical scheme to calculate the quantization condition in k-space, which is given

$$\oint (g_0 + g_1 + \cdots)dk = 2n\pi \ , \ n = 0,1,2\cdots \ . \tag{50}$$

Nnumerical evaluation of $\oint g_1(k)dk$ is required because the structure of $g_1(k)$ is not always simple.

2-4. Stabilization due to electric field

Recently, the stabilization mechanisms such as $E \times B$ mixing, poloidal shearing, resonance broadening, drift reversal and so on have been actively discussed associated with reduction of fluctuations and anomalous transport[42-45]. As an example of these mechanisms ,we here introduce the $E \times B$ sheared damping process, which was first pointed out by Timofeev[46] and then was also discussed in references[8,9]. Noting that the conventional Landau damping may be derived by the free streaming particles, which resonate with waves through the dispersion function form, $Z\left(\omega/k_{//}v_{th}\right)$. We note that the damping effect discussed here, comes from the fact that $E \times B$ sheared motion may enhance the conventional Landau damping, particularly for ions in the presence of inhomogeneous electric field. For simplicity, we consider the slab geometry and the inhomogeneity is in the x-direction. In this configuration, the drift velocity in the y-direction is given by

$$V_y \cong \frac{E_r}{B} + \frac{E_r'}{B}\frac{m}{eB}v_y \,, \tag{51}$$

where the first term gives the Doppler shift of frequency and the second term is related to the resonance. The term $\vec{k}\cdot\vec{r}'$ in the exponential part of energy integration required to derive the dispersion function is given by

$$\vec{k}\cdot\vec{r}' \approx k_{//}v_{//}t' + k_y\frac{E_r'}{B}\frac{m}{eB}v_y t' + [Oscillation\ \ term], \tag{52}$$

where we defined $\vec{r}' = \vec{r}(t')$ and the second term of rhs is the additional free streaming term perpendicular to B. Carrying out the energy integration, we finally have the modified dispersion function term, $Z\left(\bar{\omega}/\bar{k}_{//}v_{th}\right)$, where $\bar{\omega} = \omega - \bar{\omega}_{E\times B}$ and $\bar{k}_{//}^{\,2} = k_{//}^{\,2} + f(E_r')$. It should be noted that the sheared motion may modify the Landau damping process through the additional term, $f(E_r')$, the explicit form of which is given in [8,9], and the present dispersion function reduces to the standard dispersion function, $Z\left(\omega/k_{//}v_{th}\right)$ in case of no shear effect. Also, this damping still exists even though $k_{//}$ is zero.

Effect of electric field on the stability of typical modes such as drift waves[8,9],interchange modes[47] and DCLC[38] have been studied. As an example, let us show in Fig.6 the result for drift wave[9] in the bumpy torus and these theoretical prediction on the stabilizing effect of sheared $E \times B$ rotation were confirmed by experimental observation in the Gamma 10 experiment [48](see, Fig.7). In Fig.6, the growth rates normalized to the cyclotron frequency versus the normalized parameter associated with both positive and negative potential $\gamma_j = \left(\omega_{Ej}^{\ 2}/\omega_{cj}^{\ 2}\right)^2$, where $\omega_{Ej}^{\ 2} = q_j E_0/\lambda_E m_j$, are shown for several different density fraction of hot electron component. Here, we assumed a Gaussian type density profile and a parabolic potential profile, $\phi_0(x) = \left(E_0/2\lambda_E\right)x^2$. Experimental result on density fluctuation corresponding to drift mode versus γ_j is plotted in Fig.7. Although theoretical model based on the bumpy torus is different from the experiment brcause of different configuration, both results are qualitatively in agreement. We note that the most unstable situation is shifted towards negative field side(E<0), caused by the Doppler shift of frequency ,and this situation occurs when $E \times B$ drift frequency may cancel the diamagnetic drift frequency of electrons. The presence of large enough sheared rotation may enhance the Landau damping and may reduce the fluctuation level,regardless of its polarity. Similar results are reported in the biasing experiment of Tokamak de Varennes[49].

3. Reduction of Anomalous Transport due to $E \times B$ Sheared Rotation(Gradient of Electric Field Effect)

Reduction of the anomalous transport is one of the most important topics associated with the confinement improvement. As for an example of this topic, we here consider two cases: (1) reduction of anomalous transport caused by drift waves in the slab geometry , and (2) reduction of anomalous transport driven by interchange modes in toroidal helical systems. The anomalous transport in the first case may be reduced in the following two ways. The anomalous transport coefficient D derived by drift wave instabilities is estimated as $D = F\gamma k^{-2}$, where the form factor F is a numerical coefficient of order of unity[42,43]. The reduction of the growth rate due to the enhanced Landau damping mentioned in the previous section may decrease the anomalous transport(through γ - term). Nonlinear study evaluated F, and F is also reduced by the sheared rotation. One may write as $D = D_0\left(F/F_0\right)(\gamma k_\perp^{-2})/(\gamma k_\perp^{-2})_0$,where the suffix 0 denotes the value in the absence of radial electric field inhomogeneity. Therefore, we can evaluate the reduction of D due to the sheared $E \times B$ rotation compared with the case without electric field effect[50].

It is an important topic to study a possible reduction mechanism of the anomalous transport in toroidal helical systems(stellarator) because anomalous transport has been known to be the dominant loss process in this configuration. So ,we next study the second case. Recently , a better understanding of the L-mode transport in torsatron/heliotron has been achieved[51], solving the interchange -mode turbulence by the theory for the self -sustaining turbulence. We applied this formalism to analyze the self-sustaining interchange -mode turbulence in toroidal helical plasmas and derived a unified formula for the anomalous transport coefficient for the L- and H-like mode in this configuration[52]. The anomalous transport coefficient in the presence of inhomogeneous radial electric field was obtained as

$$\hat{\chi} = \left(\frac{\hat{\chi}_L}{1 + G\hat{\omega}_{E1}{}^2} \right), \tag{53}$$

which quantifies the effect of E_r' on the thermal conductivity unifying the L- and H- mode plasmas. Here, $\hat{\chi}_L$ is the anomalous transport obtained for the L-mode plasma, $\hat{\omega}_{E1}{}^2 \equiv \tau_{Ap}(mdE_r/d\hat{r})(rB)^{-1}$ and the explicit expressions of the coefficient G and other parameters are given in [52]. It turns out from eq.(53) that the suppression of the transport is prominent when $\hat{\omega}_{E1}$ is large enough, $\hat{\omega}_{E1} \approx D_0^{1/2}$,where $D_0 = \Omega' \beta' / 2\varepsilon^2$ and here, Ω' is the magnetic curvature, β' is the derivative of the beta value and $\varepsilon = a/R$. The theory also predicts the reduction of fluctuations due to $\hat{\omega}_{E1}$-effect. If we evaluate the condition for reduction for Compact Helical System(CHS) and Heliotron -E(H-E) device parameters, the reduction is expected when the gradient of E_r reaches the range of $100\mathrm{V}/_{cm^2}$,which is estimated from the condition $\hat{\omega}_E = D_0^{1/2}$. The observed value at present is approximately $10\text{-}20\mathrm{V}/_{cm^2}$, corresponding to a few percent reduction rate. Since the H-mode like confinement improvement has been observed not only in tokamaks but also in toroidal helical experiments such as W7-AS [53] and CHS[54] ,the comparison between theoretical predictions and experimental observations is one of the urgent task. As mentioned in the introduction, considerable progress on measurement technique has been made recently, then detailed analysis of electric field effect on the confinement characteristics over the whole plasma region may be realized. A couple of example on the radial structure of electric field will be discussed in Sec.6

4. Generation of Plasma Rotation (Electric Field)

As was shown in Fig. 1, neoclassical and anomalous transports, loss of energetic particles, heatings such as NBI and ECH and so on, have an influence on the generation of plasma rotation and/or electric field. In a toroidal nonaxisymmetric device like a stellarator, the electric field must be determined self-consistently from so-called ambipolarity constraint and can have a significant effect on the neoclassical transport. Lots of analytical formula[12,13,55] and numerical codes such as DKES code[56] and FPSTL code[57] have been developed to study the neoclassical transport in helical systems. In a stellarator field, or even in a tokamak toroidal field produced by finite number of coils, there is an asymmetric field component, which makes the particle orbits more complicated compared with the ones in standard tokamak configuration. The particle orbit behaves in a different way, in different regions of collision frequency such as MHD region(collisional), plateau region(intermediate), banana region(collisionless) and so on . But, the detailed discussions on these particle orbits and corresponding neoclassical transports are out of the scope of the present lecture. For example, the dependence of the diffusion coefficient in a helical configuration on the collision frequency is shown in Fig.8 [see, ref.[58]]. The difference of the diffusions of electrons and ions introduces an electric field and the transport analysis including the effect of electric field is one of the topics of the lecture. Figure 8 shows the reduction of the diffusion coefficient (D_E) due to electric field. Although a large amount of studies have been done on this topic, these discussions have not yet been completely understood, particularly in the presence of boundary layer associated with radial electric field. An numerical code based on the bounce averaged Fokker-Planck equation has been developed to solve this transport process[59]. Further improvement on these transport codes are required to analyze the boundary layer contribution in the presence of so called toroidal ($\iota v_{//}/R_0 + \omega_{E\times B} \approx 0$) and helical ($\omega_h + \omega_{E\times B} \approx 0$) resonances cased by the $E\times B$ drift motion, where ι is the rotational transform angle and $\omega_{E\times B}$ the $E\times B$ drift frequency and ω_h is the drift frequency by helical ripple.

In general, the rotation (electric field) in plasmas is determined by balancing some typical driving forces with the drag forces. There are essentially two type of forces which may enhance plasma rotations: one is the force associated with momentum transport due to, for example, neutral beam injection and the other is the bipolar fluxes caused by the ion and electron diffusions. From these considerations an example of the poloidal momentum balance equation[60], is given by

$$-e\vec{\Gamma}_{orbit} \times \vec{B} \cdot \vec{B}_p + (\vec{I}_{beam} \times \vec{B} \cdot \vec{B}_p) / area = \quad < \vec{B}_p \cdot \nabla \pi > + m_i n_i n_0 < \sigma v >_{cex} \vec{v} \cdot \vec{B}_p \quad . \quad (54)$$

The left hand side of eq.(54) is the driving forces and the right hand side means the drag forces. The first term in lhs represents the plasma ion orbit losses and the second term is the beam torque. The first term in rhs denotes the viscous drag and the second term corresponds to the neutral drag on rotating ions due to charge exchange. Based on a momentum balance equation such as eq.(54), various theoretical models to explain relatively large poloidal rotation have been proposed during past few years. As a limiting example , Itoh and Itoh[21] and Shaing and Crume[22]have discussed a L-H bifurcation theory on the basis of the poloidal momentum balance equation, namely, a balance between a torque arising from ion orbit losses(the first term of lhs) and poloidal nonlinear viscous drag(the first term of rhs). Also, Hassam[23] discussed a poloidal spin-up theory ,in which the rotation is determined by the spin-up force due to the in-out asymmetrical flux balancing with the linear viscous damping force. The thermal transport bifurcation theory[24] based on ion anomalous conductivity , which is functional of the poloidal flow, and the turbulence flow generation theory[25] have been discussed. We should note that the torque due to ion orbit losses could be a candidate as an externally controlling technique of the rotation by using ion neutral beam. The beam ions play an important role of the electrode in the biasing experiments such as Taylor's experiment[3], where they carry in electrons and then are lost to the wall in a small localized region. This localized beam current is similar to the current through electrode. Recently, the importance of the drag force due to charge exchange with neutrals has been pointed out[20,60,61].

As was shown in Fig.1, various physical processes may contribute to the generation of electric field and confinement characteristics. First, we discuss a theoretical model of self-consistent analysis to determine simultaneously the relation among the electric field, loss cone loss, and heating efficiency , particularly in stellarator and heliotron/torsatron configurations. In these configurations, the radial electric field in the steady state is evaluated by the ambipolarity condition

$$\Gamma_e = \Gamma_i \quad , \quad (55)$$

where Γ is the radial particle flux and suffix e and i denote electrons and ions, respectively. Taking into account nonclassical fluxes involved physical processes mentioned above, Γ_e and Γ_i are given as

$$\Gamma_i = \Gamma_i^{NC} + \Gamma_i^{orbit} + \Gamma_{fcx} + \Gamma_{icx} + \Gamma_{i,a} \quad , \tag{56}$$

$$\Gamma_e = \Gamma_e^{NC} + \Gamma_{e,a} + \Gamma_{RF} \, . \tag{57}$$

These equations consist of the neoclassical fluxes(denoted by the subscript NC), the direct ion orbit loss(Γ_i^{orbit}) ,the charge exchange contribution of fast ions under the influence of neutral particles (Γ_{fcx}) and bulk ions(Γ_{icx}), and that driven by anomalous transport(Γ_a). As the explicit form of Γ^{NC} , we use the formula by Kovrizhnyhh[12] and the derivations of other fluxes are discussed in [19,20], and they are summarized as

$$\Gamma_i^{orbit}(r) = \left[P(r) - P(r_*)\right] / 4\pi^2 r R W_b \quad , \tag{58}$$

$$\Gamma_{fcx} = \left(M_f n_f n_0 / eB_p\right) < \sigma_{cx} v > v_f \quad , \tag{59}$$

$$\Gamma_{icx} = \left(M n_i n_0 T_i / e^2 B^2\right) < \sigma_{cx} > \left[Ze \frac{E_r}{T_i} - \left\{1 + \eta_i \mu_{i1} / \mu_{i2}\right\} n_i' / n_i \right] \quad . \tag{60}$$

In eqs.(58)-(60), P(r) is the input power crossing the minor radius r, W_b denotes the beam energy, r_* the radius representing the loss boundary, $M_f(M)$ the fast (bulk) ion mass, $n_f(r)$ the fast ion density, $< \sigma_{cx} >$ the charge-exchange cross section, and μ_{i1} and μ_{i2} are neoclassical viscosity coefficients. As for the anomalous flux(Γ_a) is concerned, we here assume the functional form of the bipolar part of anomalous flux , $\Delta\Gamma_a \equiv \Gamma_{i,a} - \Gamma_{e,a}$ in the form

$$\Delta\Gamma_a = -\alpha_A \left(\partial n / \partial r\right) / n, \quad \alpha_A = const. \tag{61}$$

Here, the coefficient α_A is a parameter, describing the magnitude of the bipolar part of the anomalous transport, which is evaluated roughly by using experimental data of particle transport based on steady state density profile and neutral particle behavior[62]. Also,the term Γ_{RF} in eq.(57) denotes the RF- induced electron flux.

The radial electric field in the steady state is evaluated by the ambipolarity equation, eq.(55). But, we must solve not only E_r but also loss cone boundary simultaneously because of the dependence of the radius r_* in eq.(58) on the radial electric field, $r_*[E_r]$. The detailed numerical method of calculation how to determine the radial electric field and the loss rates, simultaneously has been discussed in [20]. Once the radial electric field and the loss cone boundary are determined, we can evaluate the power partition among the shine-through(η_{st}), direct orbit loss (η_{obit}), charge exchange loss(η_{cx}) and bulk heating(η_{bk}). The explicit formula is discussed in [20]. Using these expressions, the energy conservation relation is given by

$$\eta_{st} + \eta_{obit} + \eta_{cx} + \eta_{bk} = 1. \tag{62}$$

We must discuss carefully the relation between the power loss required for the enhancement of electric field due to the driving forces such as ion orbit loss and the reduction of energy loss of bulk ions through the enhancement of E_r. These evaluations may be important to conclude the over all trade-off on the energy balance.

5. Topics on Bifurcation of Poloidal Rotation

As was mentioned in the previous section, it was shown theoretically from the poloidal momentum balance equation such as eq.(54) in toroidal systems that there exist bifurcated solutions; the poloidal flow velocity can suddenly become more positive with decreasing ion collision frequency, in other words, with approaching collisionless regime. The corresponding electric field becomes more negative, suppresses turbulent fluctuations through some mechanism similar to ones discussed in subsection 2.4 , and consequently improves plasma confinement. In the standard neoclassical theory, the poloidal momentum is damped by the poloidal viscosity in case with neither sources and sinks. However, in the edge region the poloidal rotation may be driven by the torque or the viscosity associated with the ion orbit loss or any other loss channels(see, eq.(54)).

To have a relatively large rotation velocity, in other words, the transition of poloidal rotation velocity, we have to extend the validity of the expression of poloidal viscosity to the regime , $M_p \equiv U_p B/(v_t B_p) \cong 1$, where M_p is called as the poloidal Mach number and $v_t = (2T_i/M)^{1/2}$. The quantity $< B_p \cdot \nabla \cdot \vec{\pi} >$ can be calculated by solving the drift kinetic equation with mass flow velocity. The expression of poloidal viscosity in tokamaks[22] has been discussed by Shaing, who also extended this tokamak result into that in stellarator configuration[63]. These theoretical results predict that there exist one(tokamak) or more(stellarator) local maximum in the poloidal viscosity. In tokamaks, the maximum is located in the critical poloidal velocity u_{p_c} ,which is derived from $u_{pc}B/(v_t B_p) \cong 1$. On the other hand, in case of stellarator, we have two local maxima, the one is located in $M_p \cong 1$ and the other is around $M_p \cong |m - nq|/m$,where m(n) is the poloidal(toroidal) mode number and q is the safety factor. This typical result by Shaing is illustrated in Fig.9. As mentioned in the previous section(see, eq.(54)), several authors discussed a theoretical model in which the poloidal rotation can be determined the balance between a driving force arising from ion orbit loss and a drag force associated with viscosity discussed above. A simple physical interpretation of this process is that energetic collisionless particles contribute to the ion orbit loss and drive a torque, while relatively low energy collisional particles contribute to the poloidal viscosity and consequently resist the poloidal rotation.

Topic on the plasma rotation was one of the highlights during 1960's and 1970's. It was first observed by Stringer[64] that an enhancement of outward plasma diffusion takes place at a critical speed , $v_{pc} \cong \varepsilon v_{th}/q$ (ε is the inverse aspect ratio and q is the safety factor). Then, Taniuti[65] and Hazeltine et al.[66] showed that this speed is a critical speed for a stationary shock formation. This phenomenon is so called the rotation limit. During 1960's and 1970's ,as the poloidal Mach number approaches unity($|M_p - 1| \leq \varepsilon^{1/2}$), the appearance of shock -like structure in density and potential profiles has been predicted theoretically by Hazeltine et al.[66], Green[67], Asano and Taniuti[68], Stix[69] ,and Greene and Winsor[70] and others. This "slow shock" formation has been observed in toroidal devices , for example, l=3 stellarator such as B-3[71] and JIPP-1[72]. It is also pointed out theoretically that "strong shock" may be formed when the rotating velocity is close to the critical one ($|M_p - 1| << \varepsilon^{1/2}$)[73, 74]. We should note that the poloidal viscosity tends to infinity if we evaluate the viscosity by using the solution derived from linear theory because the viscosity is proportional to the gradient of density and/or potential, then these quantities become infinity just at the shock front which is located at the critical poloidal angle. Interesting topics associated with plasma rotation phenomena are reviewed recently in [75].

Let us revisit the past experiments on plasma rotation in B-3 and JIPP-1 stellarators. In the B-3 stellarator experiment, the radial electric field was firstly derived by positively biased Langmuir probe and the relationship between electric field and plasma confinement was studied. This experiment showed that the increasing imposed radial electric field improved the confinement but further increase degrades the confinement as the imposed electric field was over the critical value. This fact was investigated in this experiment by adjusting the magnitude of magnetic field. It was confirmed that the critical value of electric field was qualitatively in agreement with the condition, $M_p \cong 1$. Similar plasma rotation experiment was carried out in the JIPP-1 stellarator by the electron injection into an afterglow plasma to raise the plasma rotation, in other word, to realize the plasma spin-up. This experiment revealed that the steady shock-like structure in the density and potential profiles was formed near the critical rotation velocity and the confinement degraded again as the rotation speed is large enough. It should be noted that this experiment was carried out in the Xenon plasma, where the situation $M_p \cong 1$ was easily realized even for relatively slow level of rotation velocity. These experimental observations are contradictory to the theoretical predictions in tokamaks. The study on whether these results for L=3 stellarators have something in common with that for L=2 helical devices or not , is one of attractive and urgent topics associated with confinement improvement.

Let us introduce briefly a theoretical result associated with shock solution in a poloidally rotating tokamak plasma [73,74]. When the Mach number M_p of the poloidal rotation in a tokamak approaches unity, the poloidal variations of plasma density and potential appear to have the characteristics of a shock whose front lies on a plain of a fixed poloidal angle η_0 . The shock first appears when $|M_p - 1| \leq \varepsilon^{1/2}$ on the inside of the torus at the angle $\eta_0 \geq \pi$ if the plasma rotates counterclockwise poloidally. As M_p increases, η_0 moves in the direction of the poloidal rotation. At $M_p \cong 1$, $\eta_0 = 2\pi$. When $|M_p - 1| << \varepsilon^{1/2}$, the shock angle is at $\eta_0 \leq \pi$. A schematic diagram for the solution (potential variation) versus angle η as the poloidal rotation velocity changes is shown in Fig. 10. In this figure, (a) and (c) represent the slow shock solutions and (b) corresponds to the strong shock solution. Numerical results of the slow shock solution for density variation similar to (a) and (c) were discussed in [70]. Using these shock solutions, the poloidal viscosity at $M_p \cong 1$ was evaluated by a nonlinear analysis[73]. This analysis showed that the viscosity reaches the local maximum at $M_p \cong 1$, which is the barrier that must be overcome to have a poloidal supersonic flow.

6. Electric Field Structure in Helical Devices

Although understanding of the physics associated with electric field is one of the current topics in tokamaks as well as in stellarators and heliotron/torsatrons, we here restrict our discussions to the stellarator and torsatron cases. As for the classification of typical devices and their machine and plasma parameters, refer to the lecture by Fujiwara[76]. As mentioned in Sec.4 , both neoclassical theories and transport codes in these devices are actively discussed , suggesting that an electric field reduces the helical ripple loss, and consequently improves the confinement. The relationship among electric field, fluctuations and plasma confinement was studied in the past stellarator experiments. These experiments have led to a qualitative understanding, but quantitative results have been lacking due to the difficulty of measurement technique. The poloidal rotation has been measured by using the intrinsic impurity radiation in the WVII-A[5] and Heliotron -E (H-E)[6]. However, the measurements are limited only near the plasma periphery in these experiments. A progressive measurement with improved time and spatial resolution is required to get a data in the whole plasma region. In the Compact Helical System(CHS) , the electric field profile in the whole plasma region has been evaluated from both toroidal and poloidal rotation velocities and pressure gradient by using CXS. In the CHS , the electron temperature and density profile are measured with Thomson scattering. The ion temperature and toroidal as well as poloidal rotation profiles are measured by CXS. Then, the radial electric field profile is evaluated by the force balance equation for impurities

$$E_r = \left(\partial P_I / \partial r\right) / eZ_I n_I - \left(B_\theta U_\phi - B_\phi U_\theta\right) , \tag{63}$$

where the suffix I stands for the measured impurity species. It should be noted that the radial frictional force between different species is small enough to be neglected. Recently, a heavy ion beam probing(HIBP) has been constructed with a new idea to manage complicated probing beam trajectories in the CHS. With this method, we succeeded to measure directly the radial profiles of electrostatic potentials(or electric field) over the whole plasma region[77].

As was mentioned in Sec.4, there are two type of forces to drive the plasma rotation, i.e., forces associated with momentum balance equation and ambipolar relation. The physical mechanism and mutual relations to determine the electric field in toroidal plasmas are shown schematically in Fig.11. Both experimental and theoretical studies to control the electric field have been actively discussed in connection with the recent CHS experiments. Particularly, many

experimental approaches to control the electric field have been done,by adjusting the neutral beam injection, by controlling ion and electron loss channels with NBI and/or ECH , due to biasing technique and so on. Next, the comparison between theoretical predictions and experimental observations in typical stellarator experiments has been made. Analysis based on the ambipolar condition,eq.(55) is applied to the NBI and ECH heated plasmas in CHS and WVII-A. Typical machine and plasma parameters for CHS and WVII-A are summarized in [78,79]. Sample distributions of density and temperatures, stimulating the experimental results in these two devices, are shown in Fig.12a for CHS and in Fig.12b for WVII-A. The WVII-A stellarator is characterized by an weak helical ripple, $\varepsilon_h << r/R$ (r and R are the minor and major radius, respectively). It should be noted that the poloidal gyroradius of fast ions generated by NBI is compatible with the minor radius, and the trapping is very difficult without the help of radial electric field in the WVII-A configuration , in other words, the radial electric field has a strong influence on energetic particle confinement[80]. On the other hand, one of the key features of the CHS device is that the magnetic field configuration of this type of device is controllable by adjusting the poloidal field coil current. The observed E_r profile for fixed density and temperatures(Fig.12a) is shown in Fig.13, together with the neoclassical results calculated from the neoclassical formula by Kovrizhnykh[12] and Hastings[13]. It was found from the comparison that the observed E_r deviates from the neoclassical prediction and the results for both low and high density NBI operations were far from satisfactory. Therefore, some other large ion loss channel is required to explain this discrepancy. We carried out a selfconsistent analysis for cases of various type of operations in these two devices ,based on the theoretical model discussed in Sec.4, which determines the loss of energetic particle (fast ions) and electric field, simultaneously. Numerical result of the radial electric field profile in WVII-A is shown in Fig.14 for given parameters[79]. In Fig.14, the solid line is the selfconsistent solution for electric field under the influence of fast ion loss. Lines with(1) and (2) indicate the case of the beam energy W_b = 14keV and 28keV, respectively. Dotted line is for the neoclassical prediction and solid circles indicate the experimental observations. The radial profile in the region of r< 1/2 may be determined by the neoclassical process and the effect of ion orbit loss is substantial near the plasma edge. The enhancement of radial electric field due to fast ion orbit loss is found in the peripheral region, which is effective in confining about 1/2 of the injected fast ions in spite of the loss of about 10% of born particles. The partition of the injection power(1.2MW, 14keV) evaluated based on eq.(62) is given as

$$\eta_{st} : \eta_{orbit} : \eta_{bk} = 0.49 : 0.04 : 0.47 . \qquad (64)$$

To explain the deviation of theoretical result from experimental observation shown in Figs. 13 and 14 , the effect of the neutral particles on the electric field was examined,by keeping the third term of rhs of eq.(56). It turns out from these analyses that the electric field becomes more negative at the plasma edge in the presence of neutral particle contribution. Associated with this increment of the radial electric field, the ratio of the orbit loss is reduced, but the increment of the charge exchange loss is much larger than this reduction. So, this clearly shows that the enhancement of electric field by using the fast ion loss is not useful so long as one considers the neoclassical energy loss process. The effect of fast ion orbit loss on E_r is also investigated in the NBI experiment of CHS, for the given profiles and parameters shown in Fig. 12a. This analytical result indicates that the fast ion orbit loss caused by the loss cone makes E_r more negative, but the influence of the orbit loss appears only in the plasma edge. This theoretical prediction has been confirmed in the NBI heating experiment with variable injection angle[81]. Since the difference between theoretical results and experimental observations still exists particularly in the region of $0.5a<r<0.8a$, another ion loss process in addition to orbit loss , is necessary to explain this discrepancy. Therefore, the effect of the following two loss processes on E_r in addition to NC loss and orbit loss are studied : (1) effect of charge exchange loss of fast ions with neutral and (2) effect of bipolar part of anomalous particle loss. In these studies, we note that the neutral hydrogen profile in core plasma region and the toroidal/poloidal distributions in the recycling area near the inner wall were measured by a calibrated TV camera and a laser- induced fluorescence method[82]. As for the neutral density and fast ion particle distributions, we assume the following sample distributions:

$$n_0(\rho) = n_{0s}\exp[-\alpha_0(1-\rho)^2], \tag{65}$$

$$n_f(\rho) = n_{0f}\exp[-\alpha_f\rho^2] \ , \tag{66}$$

where the profile fitting parameter α_0 is evaluated by the DEGAS code based on experimental data ($\alpha_0 \cong 10$) but there is no data for fast ion distribution and we assumed a broad profile by choosing $\alpha_f \cong 2$. Also, the anomalous particle loss was evaluated on the basis of the local particle transport experiment for NBI heated plasma[62]. Figure15 shows the radial profile of electric field for different values of α_A and neutral density at the edge n_{0s} is fixed to be $5.0\times10^{17}/m^3$ for low density and $1.5\times10^{18}/m^3$ for high density cases, respectively. Open and closed data points are the experimental values. It was found that both neutral particle contribution

and anomalous particle loss further enhance the radial electric field and may reproduce the experimental results by adjusting the parameters. But, the required neutral density seems to be higher than the experimental observations[82]. Also, it should be noted that the data on neutral density and other parameters have not obtained simultaneously in these experiments.

In order to certify the dependence of radial electric field, particularly, the polarity dependence on the confinement, it is necessary to control the electric field externally. Recently, a transition of an electric field from negative to positive has been studied in the superposition experiment of ECH on NB heated plasma in CHS. These experiments have been done by enhancing the electron particle flux associated with the accelerated energetic electrons produced by the second harmonic ECH and the mutual relationship among resonance positions(ripple top or ripple bottom), power and injection modes were also studied[83]. Figure 16 shows the radial profiles of radial electric field at 15ms after the ECH is turned on for the reference plasma(NB heated plasma without ECH by keeping the same line-averaged density as that for the plasma with ECH) and those with $P_{ECH} = 85kW$ and 140kW. Relatively large positive electric field is observed in case of 140kW while the radial electric field for the reference plasma and that with 85kW is almost zero or small negative value. The relationship between the polarity of electric field and the confinement improvement has been studied, but experimental evidence has not been obtained[27]. Further studies at the lower collisionality region would be required to get the final conclusion. Direct experimental observations of potential profile in CHS have been carried out by using 200keV heavy ion beam probe, giving improved database on fine structure of potential profile over the whole plasma region[77]. Figure 17 shows radial electric field profile deduced from polynomial fitting curves to the obtained potential profile. In the ECH plasmas, the positive electric field turns more negative as the density increases. In the medium density operation, the electric field shows a strong shear at the periphery. Experimentally obtained electric field can be compared with the result predicted by the ambipolarity condition, (55). The theoretically expected electric field has a similar tendency to the experimental observation in this case. After the applicable region of the HIBP is extended to higher density discharges by reinforcing the power supply capacity, simultaneous measurement of the electric field profile(HIBP) and impurity velocity(CXS) will allow to give a new insight to impurity transport.

Finally we explain a plasma rotation drive experiment by an electrode discharge in helical devices. As discussed in the previous section, a couple of experiments have been done to overcome the rotation barrier in the L=3 stellarators and these results showed the improvement of the confinement in the slow rotation phase but the degradation in the fast rotation phase.

We challenged similar experiment in the CHS [84]. These experiments showed that radial current cased by electrode discharge enhanced the poloidal rotation but the rotation velocity did not reach the bifurcation point $M_p \cong 1$(the value M_p is around 0.3 to 0.5 in this experiment). In helical configurations, in general , plasma hardly rotates compared with tokamak case because the damping force due to viscosity caused by helical ripples is larger than that in tokamaks. Therefore, a novel idea to realize more radial current is required to overcome this difficulty.

7.Summary

In the present lecture, we surveyed theoretical and experimental topics associated with radial electric field generation process and its influence on stability and transports in toroidal plasmas. First, the stability theories to analyze typical modes in an inhomogeneous plasma were discussed on the basis of both fluid and kinetic descriptions . The WKB mode analysis based on both second order differential equation and integral equation in k-space were reviewed . Reduction of anomalous transport due to sheared rotation(gradient of electric field) was also discussed. We next studied theoretical modeling on selfconsistent analysis in determining radial electric field and loss cone loss particularly , in heliotron/torsatrons under the influence of nonclassical ion losses such as loss cone loss of fast ions, charge exchange loss of fast ions with neutrals and bipolar part of anomalous transport. Topics on bifurcation phenomena of plasma rotation such as shock solution and transport barrier were briefly reviewed. Current experimental observations on electric field structure in NBI, ECH and biased plasmas in helical devices(CHS and WVII-A) were surveyed, and comparison between theoretical predictions and observations on radial electric field structure were made in these experiments.

Acknowledgements

The author wish to acknowledge Drs. K. Itoh, J. Todoroki, T. Kamimura , S.-I. Itoh, K.C.Shaing, R. D. Hazeltine, K. Ida, H. Idei, H. Iguchi ,A. Fujisawa , H. Yamada and all group members of torus experiment in NIFS for close collaborations and stimulating discussions on the present topics associated with electric field. The author thanks Drs. J. Weiland and C.S.Liu for fruitful discussions on wave analysis based on fluid equations and also thanks Drs. T. Watanabe, R. Ferraro, B. D. Fried and R. Littlejohn for valuable discussions and collaborations on WKB analysis based on integral equation in k-space.

References

[1] R. J. Groebner et al., Phys. Rev. Lett. 64 (1990)3015.

[2] K. H. Burrell et al. , Phys. Fluids B2 (1990)1405.

[3] R. J. Taylor et al. ,Phys. Rev.Lett. 63 (1989)2365.

[4] K. Ida et al. ,Phys. Rev.Lett. 65 (1990)1364.

[5] H. Wobig, H. Massberg, H. Renner, The WVII-A Team, in Plasma Physics and Controlled Nuclear Fusion Research, 19866, 11th Int. Conf. Kyoto,1986(IAEA Vienna 1987) Vol.2 p.369.

[6] K. Kondo et al. , in Proc. of Int. Conf. on Plasma Physics, Innsbruck, Austria, 1992, Vol.16C, Part I, p529.

[7] K. Matsuoka et al. , in Proc. of Plasma Physics and Controlled Nuclear Fusion Research, 1988, Nice, France(IAEA Vienna Austria 1989), Vol.II, p411.

[8] H. Sanuki, T. Watanabe and M. Watanabe, 23 (1980)158.

[9] H. Sanuki, Phys. Fluids 27 (1984)2500.

[10] K. C. Shaing, E. C. Crume Jr. and W. A. Houlberg, Phys. Fluids B2 (1990)1492.

[11] G. M. Staebler and R. R. Dominquez, Nucl. Fusion 31 (1991)1891.

[12] L. M. Kovrizhnykh, Nucl. Fusion 24 (1984)435.

[13] D. E. Hasting, W. A. Houlberg and K. C. Shaing, Nucl. Fusion 25 (1984)445.

[14] K. Itoh, S.-I. Itoh, A. Fukuyama, H. Sanuki and M. Yagi, Plasma Phys. Control. Fusion 36 (1994)123.

[15] K. Itoh, S.-I. Itoh, A. Fukuyama, M. Yagi and H. Sanuki, Trans. of Fusion Tech. 27, (1995)52.

[16] F. Wagner et al., Phys. Rev. Lett. 49 (1982)1408.

[17] K. H. Burrell et al. , Phs. Fluids B2, (1990)1405.

[18] R. R. Weynants and R. J. Taylor , Nucl. Fusion 30 (1990)945.

[19] H. Sanuki, K. Itoh, K. Ida and S.-I. Itoh, J. Phys. Soc. Jpn. 60 (1991)3698.

[20] H. Sanuki , K. Itoh and S.-I. Itoh , J. Phys. Soc. Jpn. 62 (1993)123.

[21] S.-I. Itoh and K. Itoh, Phs. Rev. Lett. 60,(1988)2279.

[22] K. C. Shaing and E. C. Crume Jr., Phys. Rev. Lett. 63 (1989)2369.

[23] A. B. Hassam et al. , Phys. Rev. Lett. 66 (1991)309.

[24] F. L. Hinton, Phys. Fluids B3 (1991)696.

[25] P. H. Diamond and Y.-B. Kim , Phys. Fluids B3 (19911626.

[26] K. Ida and S. Hidekuma , Rev. Sci. Instrum. 60 (1989)876.

[27] K. Ida et al. , Jpn. Soc. of Plasma Science and Nucl. Fusion Res. Vol. 70 (1994)514 (in Japanese), NIFS Report-313(1994).
K. Ida et al. ,Phys. Fluids B3 ,(1991)515, B4, (1991)1533.
[28] see, IEEE Trans. Plasma Science Vol. 22 (1994),Special Issue On Heavy Ion Beam Probing,which is edited by K. A. Connor and T. P. Crowley.
[29] A. Fujisawa et al. ,Rev. Sci. Instrum. 63 (1992)3694.
[30] S. Sasaki et al.. , Plasma Physics 1 (1994)1089.
[31] J. Weiland, H. Sanuki and C. S. Liu, Phys. Fluids 24 (1981)93.
[32] A. Hasegawa and M. Wakatani, Phys. Fluids 26 (1983) 2770.
[33] J. N. Davison and T. Kammash, Nucl. Fusion 8 (1968) 203.
[34] T. Watanabe, H. Sanuki and M. Watanabe, J. Phys. Soc. Jpn. 47 (1979) 286.
[35] M. Watanabe et al., J. Phys. Soc. Jpn. 50 (1981) 1738.
[36] T. Watanabe et al., J. Phys. Soc. Jpn. 50 (1981) 1745.
[37] G. R. Burkhart, P. N. Guzdar and R. G. Littlejohn, Phys. Fluids 31 (1988)2928.
[38] H. Sanuki and R. D. Ferraro, Physica Scripta 34 (1986) 58.
[39] R. D. Ferraro, H. Sanuki, R. G.Littlejohn and B. D. Fried, Phys. Fluids 28 (1985)2181.
[40] R. D. Ferraro, R. G.Littlejohn ,H. Sanuki and B. D. Fried, Phys. Fluids 30 (1987)1115.
[41] H. L. Berk and D. Pfirsh, J. Math. Phys. 21(1980) 2054.
[42] H. Bigrali, P. H. Diamond and P. W. Terry, Phys. Fluids B2 (1990) 1.
[43] K. C. Shaing, Comments on Plasma Contr. Fusion 14 (1991) 41.
[44] H. Sugama and M. Wakatani, Phys. Fluids B3 (1991) 1110.
[45] S.-I. Itoh and K. Itoh, J. Phys. Soc. Jpn. 59 (1990) 3815.
[46] A. V. Timofeev, Sov. Phys. Tech. Phys. 11 (1967) 1331.
[47] H. Sanuki, J. Phys. Soc. Jpn. 52 (1983) 511.
[48] A. Mase et al., Phys. Rev. Lett. 64 (1990) 2281.
[49] A. Boileau et al., Nucl. Fusion 32 (1992) 995.
[50] S.-I. Itoh, H. Sanuki and K. Itoh, J. Phys. Soc. Jpn. 60(1991) 2505.
[51] K. Itoh, S.-I. Itoh and A. Fukuyama, Phys. Rev. Lett. 69 (1992) 1050.
[52] K. Itoh, S.-I. Itoh, A. Fukuyama, H. Sanuki and M. Yagi, Plasma Phys. Contl. Fusion 36(1994) 123.
[53] V. Erckmann et al., Phys. Rev. Lett. 70 (1993) 2080.
[54] K. Toi et al., Proc. 14th Int. Cof. on Plasma Physics and Controlled Nuclear Fusion Research (Wurzburg, 1992) paper H-1-3.

[55] K. Miyamoto, Nuclear Fusion 18 (1978)243.
[56] S. P. Hirshmann et al., Phys. Fluids 29 (1986)2951.
[57] H. E. Mynick and W. N. G. Hitchon , Nuclear Fusion 26 (1986) 425.
[58] J. T. Lacatski, W. T. Houlberg and N. A. Uckan, ORNL Research Report, ORNL/TM-9533(1985).
[59] J. Todoroki and H. Sanuki, to be published in Proceeding of the 1996 International Conference on Plasma Physics, (9-13 Sept. 1996, Nagoya).
[60] T. Ohkawa and R. L. Miller , in 13th Int. Conf. on Plasma Physics and Controlled Fusion Research(IAEA, Washington, 1990) IAEA-CN-53/A-7-11.
[61] K. C. Shaing et al. , in 12th Int. Conf. on Plasma Physics and Controlled Fusion Research(IAEA, Nice, 1988)Vol. 2, p.13.
[62] H. Iguchi et al. , in Proc. 1992 Int. Conf. on Plasma Physics and 19th European Conf. on Controlled Fusion and Plasma Physics(Innsbruck, Austria) Part1 ,p517.
[63] K. C. Shaing, Phys. Fluids B5 (1993) 3841.
[64] T. E. Stringer, Phys. Rev. Lett. 22 (1969) 770.
[65] T. Taniuti, Phys. Rev. Lett. 21 (1970) 1478.
[66] R. D. Hazeltine , E. P. Lee and M. N. Rosenbluth, Phys. Fluids 14(1971)361.
[67] B. J. Green, Nuclear Fusion 12(1972)475.
[68] T. H. Stix, Phys. Fluids 16(1973)1260.
[69] N. Asano and T. Taniuti, Phys. Fluids 16(1973)1239.
[70] J. M. Greene and N. K. Winsor, 16(1973)863.
[71] J. G. Gorman and L. H. TH. Rietjents , Phys. Fluids 9 (1966)1504.
[72] A. Mohri and M. Fujiwara , Nucl. Fusion 14, (1974)67.
[73] K. C. Shaing, R. D. Hazeltine and H. Sanuki, Phys. Fluids B4 (1992) 404.
[74] T. Taniuti et al., J. Phys. Soc. Jpn. 61 (1992) 568.
[75] V. Rozhansky and M. Tendler, *Plasma rotation in Tokamaks* ,Rev. of Plasma Physics edited by B.B. Kadomtsev, Vol. 19, pp147 .
[76] M. Fujiwara, see the lecture note in the Asian Science Seminar(1996, October, Hefei).
[77] A. Fujisawa et al. , in 16th Int. Conf. on Plasma Physics and Controlled Fusion Research(IAEA, Montreal, Canada, 1996) IAEA-CN-64/C1-5.
[78] H. Sanuki et al., Physica Scripta 52 (1995) 461.
[79] U. Stroth et al. , Nucl. Fusion 36 (1996) 1063.

[80] K. Itoh, H. Sanuki and S.-I. Itoh, J. Phys. Soc. Jpn. 61(1992)2294.
[81] S. Okamura et al., in 14th Int. Conf. on Plasma Physics and Controlled Fusion Research(IAEA, Wurzburg, Germany, 1992) IAEA-CN-56/C-2-4.
[82] K. Uchino et al. , J. Nuclear Materials 196-198(1992) 210.
[83] H. Idei, K. Ida , H. Sanuki et al. , Phys. Plasmas 1, (1994)3400.
[84] H. Yamada et al., in the Proc. Japan Society of Plasma Science and Nuclear Fusion Research Meeting(1992, Ohsaka Univ.) pp143.(in Japanese)

Figure Captions

Fig.1 Mutual relationship among physical processes associated with electric field.

Fig.2 The curve C , Anti-Stokes lines for function Q(z) with two turning points z_1 and z_2 ,and Branch cuts are plotted in Fig.1a . The form of the solution of eq.(25) is roughly illustrated(quoted from ref.33).

Fig.3 Schematic Plot of g=g(k) for a spatially localized mode. The turning points in x-k space are also indicated by x_{ij} and k_{ij} (j=1,2). This is quoted from ref.34.

Fig.4 Results for $\tilde{g}_0(\tilde{k})$ for given values of ω_r/ω_{*i} are shown. The parameters are $\omega_{pi}^2/\omega_{ci}^2 = 100$, $T_i/T_e = 1.0$, $\lambda/\rho_i = 10^2$, and $k_{//}\rho_i = 10^{-3}$. (a) $k_\perp\rho_i$=0.4, (b) 0.8, and (c) 1.2. This result is quoted from ref.8.

Fig.5 Results of ω_r/ω_{*i} (the solid line) and ω_i/ω_{*i} (the dotted line) vs $k_\perp\rho_i$ for the radial mode number n=1-6 are illustrated in case of a cesium plasma. The parameters are $\omega_{pi}^2/\omega_{ci}^2 = 100$, $T_i/T_e = 1.0$, $\lambda/\rho_i = 10^2$ and $k_{//}\rho_i = 10^{-3}$. This is quoted from ref.8.

Fig.6 The maximum growth rates of the N=0 and N=1 drift modes in the presence of hot electron component with density fraction 10% (N is the radial mode number) ,which are denoted by the dotted lines, versus both the positive and negative ambipolar potential ($\pm\gamma_i$). The maximum growth rate of the fundamental mode (N=0) without hot electron component is also shown by the solid line(quoted from ref.9).

Fig.7 Fluctuation level of drift wave as a function of ampipolar field(quoted from ref.48).

Fig.8 Particle diffusion coefficient D versus electron collision frequency ν_e . Illustrated are the Pfirsch-Schluter(SP), plateau(P), helically trapped(H), helical plateau(HP), supperbanana (SB), and collisionless detrapping(E) regimes. Transition frequencies between these collisionality regimes are also shown(equated from ref.58).

Fig. 9 Controlling the relative magnitude of ε_h and ε_t , the toroidal maximum can be made either larger or smaller than the helical maximum. This is quoted from ref.63.

Fig.10 Variation of potential versus angle η for three different values of Mach number M_p. As M_p increases, the shock angle varies from $\pi < \eta_0 < 2\pi$ for $1 - M_p \leq \varepsilon^{1/2}$ (a) to $\eta_0 = 2\pi$ for $M_p \cong 1$(b) and to $0 < \eta_0 < \pi$ for $M_p - 1 \leq \varepsilon^{1/2}$ (c). This result is quoted from ref.73.

Fig.11 Physical mechanism and mutual relations to determine the electric field in toroidal plasmas.

Fig.12 Density and temperature profiles are shown in (a) for CHS and (b) for W7-A. These results are quoted from ref.20 and ref.80.

Fig.13 The observed E_r profile of the low and high density NBI experiment in CHS is plotted for fixed density and temperature as was shown in Fig.12, together with the neoclassical results evaluated from neoclassical transport theory by Kovrizhnykh(ref.12) and Hastings et al.(ref.13).

Fig.14 Numerical results of electric field profile in W7-A are shown. Solid lines are the selfconsistent solutions under the influence of fast ion orbit loss. (1) and (2) correspond to the cases of beam energy, 14keV and 28keV, respectively(quoted from ref.80).

Fig.15 Radial profile of E_r for several values of α_A ; (a) $\alpha_A = 0$, (b)5×10^{18}, (c) 1.0×10^{19}, and $n_{0s} = 5.0 \times 10^{17} / m^3$ in (A) and $1.5 \times 10^{18} / m^3$ in (B) are used. The results for low density and high density are shown in (A) and (B), respectively. Open and closed data points are the experimental results. These results are quoted from ref. 27.

Fig.16 Radial profile of the electric field for the discharges without and with ECH(85kW and 140kW) in CHS heliotron/torsatron(see, Fig.12 of ref.27 or ref.83).

Fig.17 Electric field profiles in the steady states of ECH and NBI plasmas. The expected electric field profile from the neoclassical theory is presented by a dotted line for comparison (ref.83).

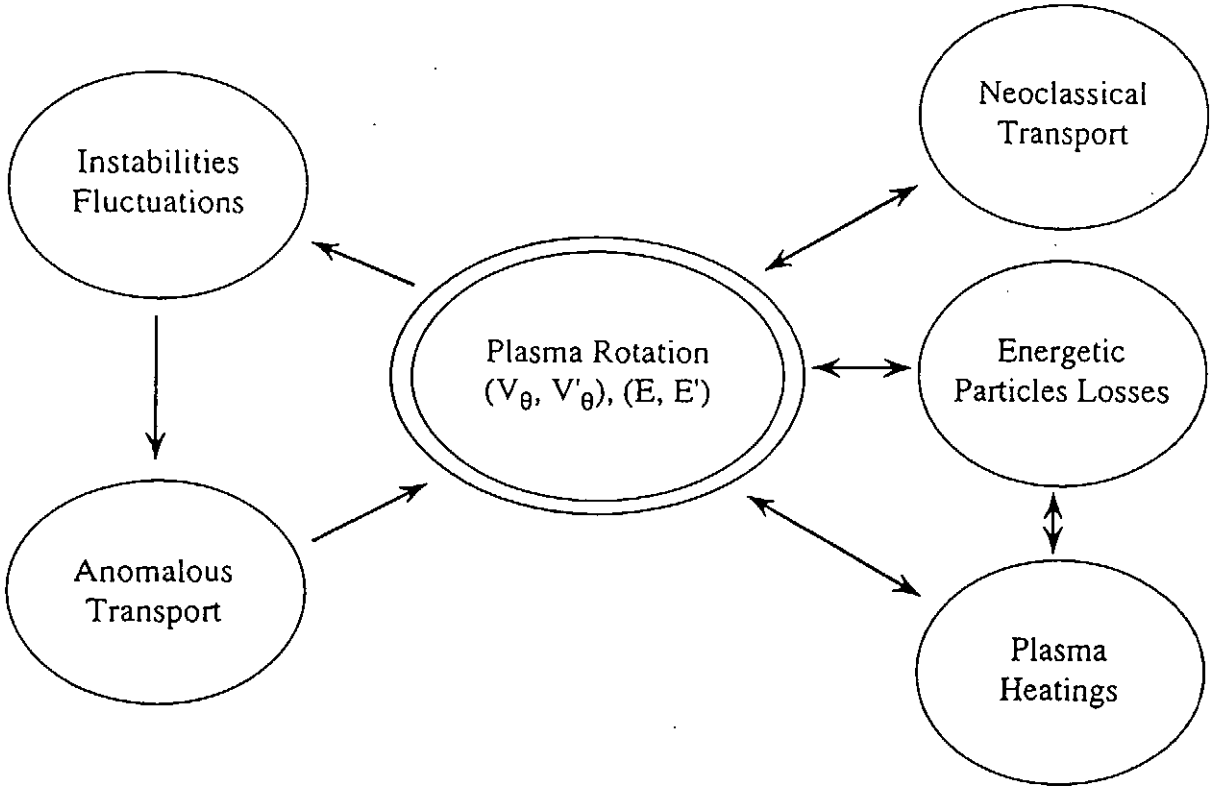
Instabilities
Fluctuations
Neoclassical
Transport
Plasma Rotation
(V_θ, V'_θ), (E, E')
Energetic
Particles Losses
Anomalous
Transport
Plasma
Heatings

Fig.1

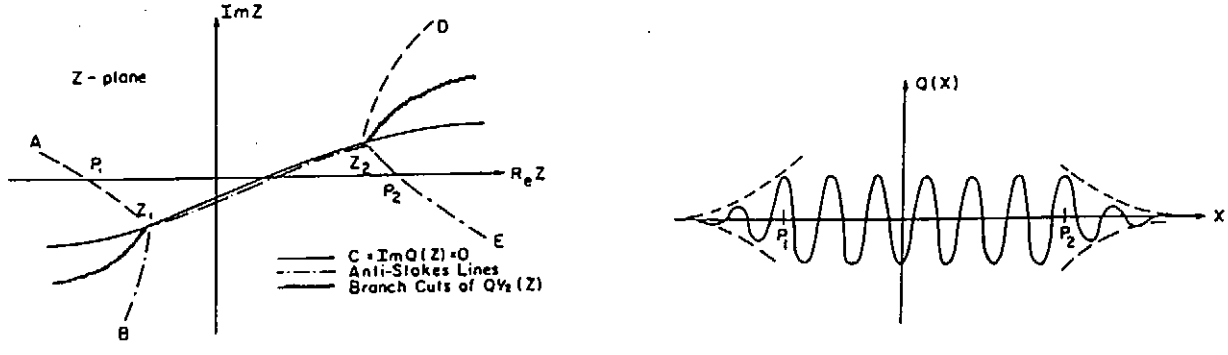
ImZ
Z - plane
D
A
P_1
Z_2
R_eZ
Z_1
P_2
E
B
C = ImQ(Z) = 0
Anti-Stokes Lines
Branch Cuts of $QV_2(Z)$
Q(X)
X
P_1
P_2

Fig.2

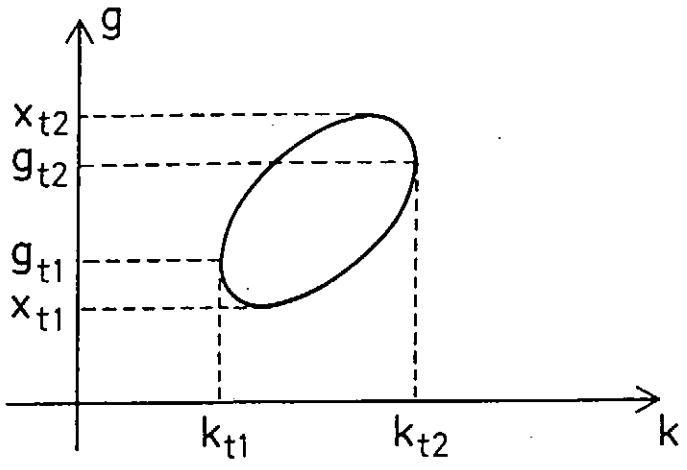

Fig.3

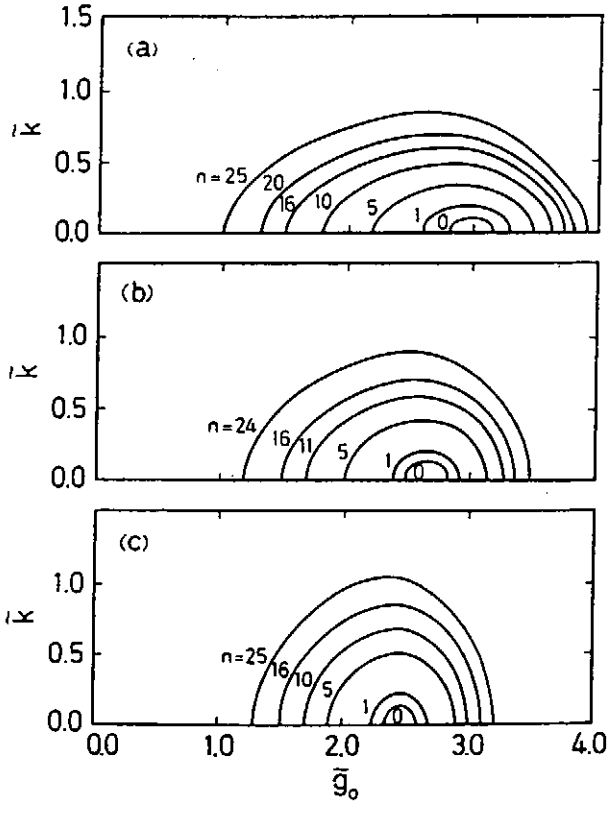

Fig.4

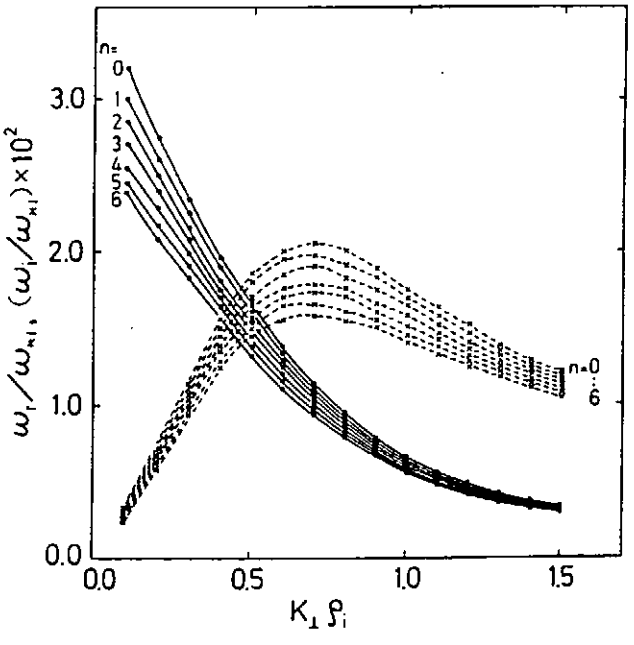

Fig.5

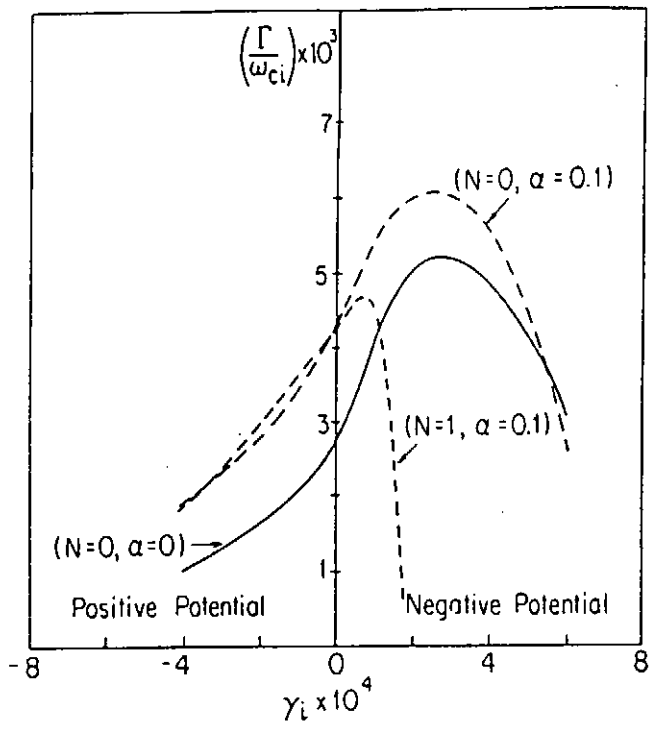
$\left(\frac{\Gamma}{\omega_{ci}}\right)\times10^3$
7
5
3
1
(N=0, α=0.1)
(N=1, α=0.1)
(N=0, α=0)
Positive Potential
Negative Potential
-8
-4
0
4
8
$\gamma_i \times 10^4$

Fig.6

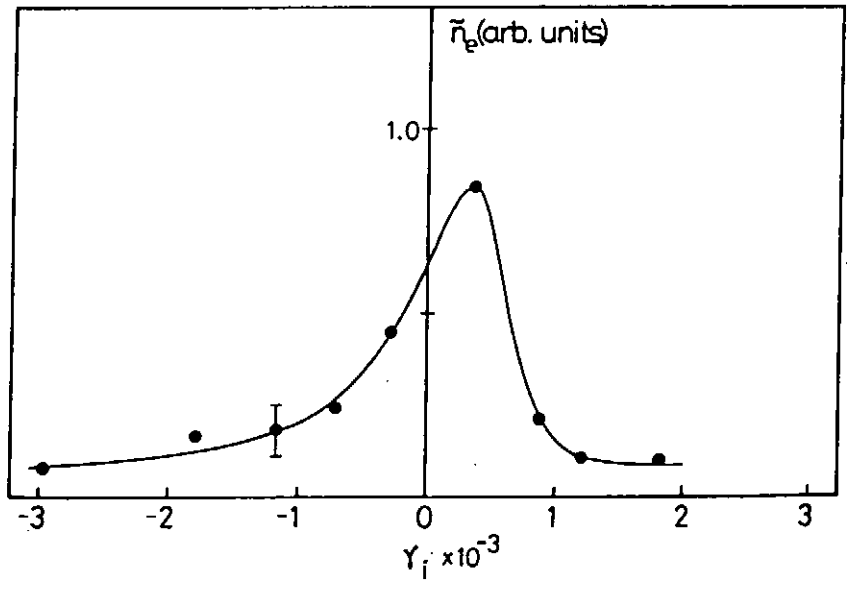
$\tilde{n}_e$(arb. units)
1.0
-3
-2
-1
0
1
2
3
$\gamma_i \times 10^{-3}$

Fig.7

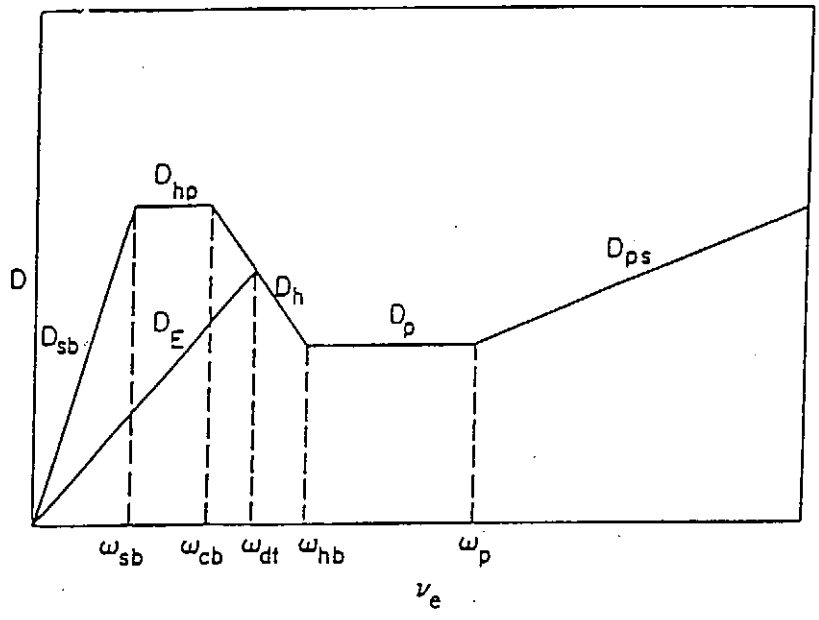
D
D_{hp}
D_{sb}
D_E
D_h
D_p
D_{ps}
ω_{sb}
ω_{cb}
ω_{dt}
ω_{hb}
ω_p
ν_e

Fig.8

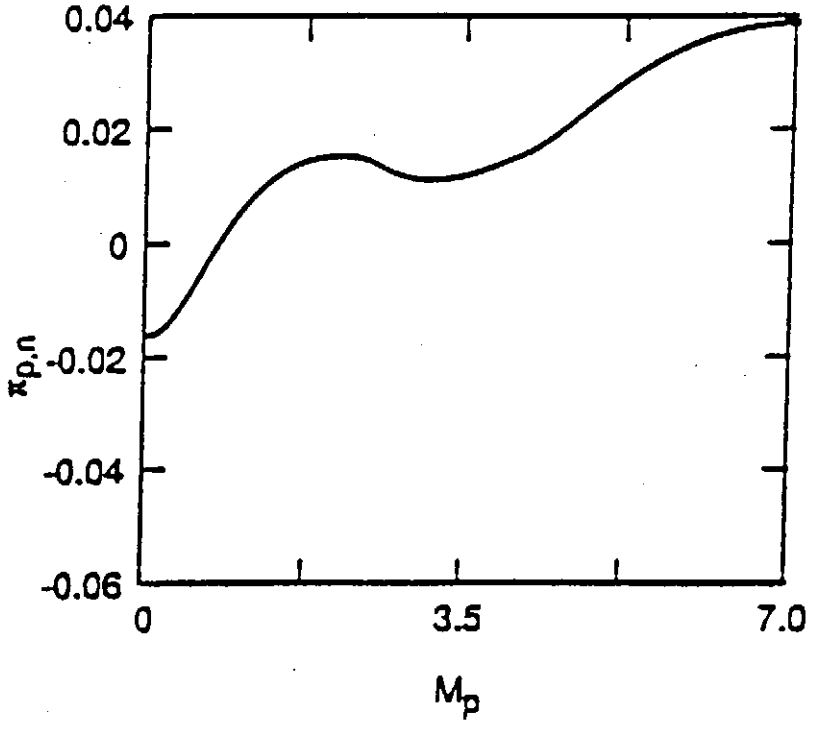
0.04
0.02
0
-0.02
-0.04
-0.06
$\pi_{p,n}$
0
3.5
7.0
M_p

Fig.9

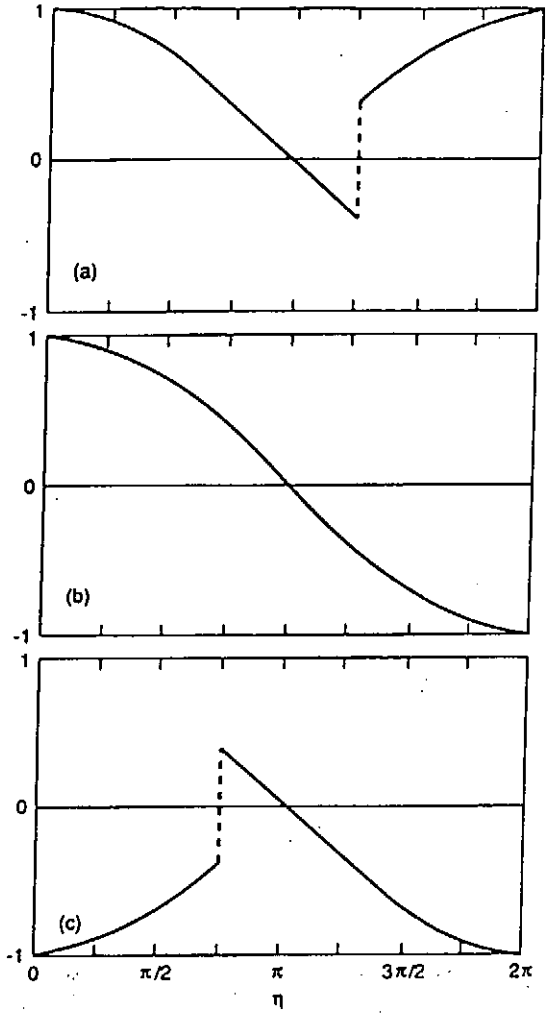
1
0
-1
(a)
(b)
(c)
0
π/2
π
3π/2
2π
η

Fig.10

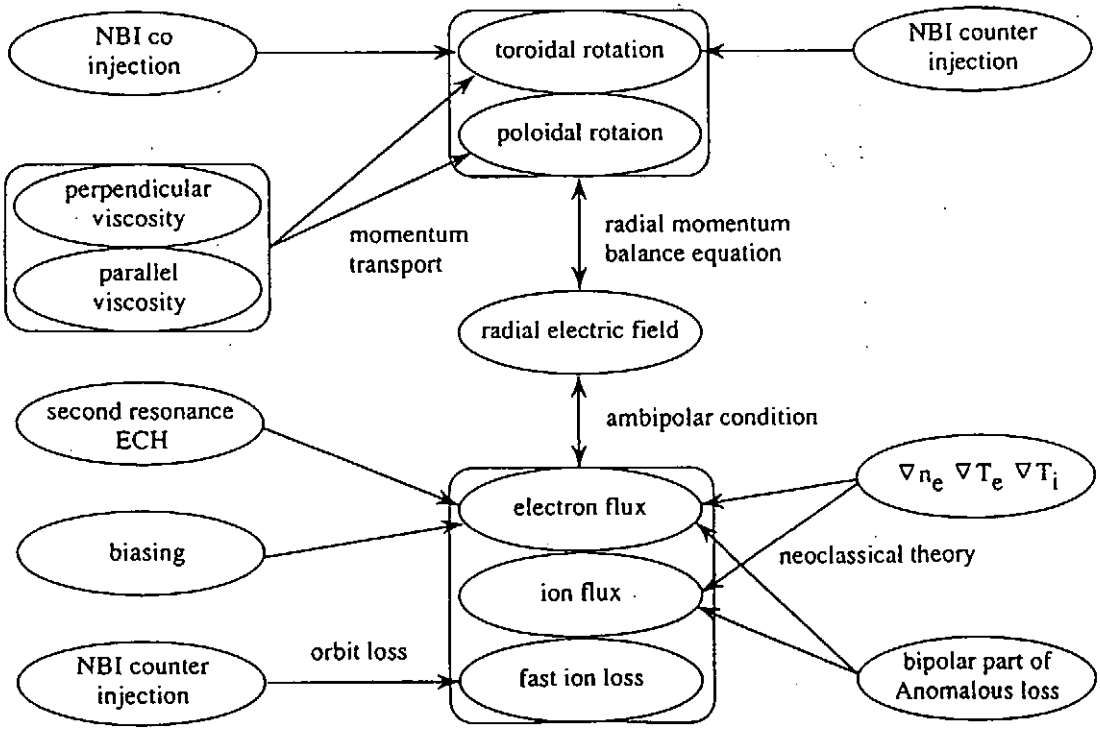
NBI co injection
toroidal rotation
NBI counter injection
poloidal rotaion
perpendicular viscosity
parallel viscosity
momentum transport
radial momentum balance equation
radial electric field
second resonance ECH
ambipolar condition
electron flux
∇n_e ∇T_e ∇T_i
biasing
neoclassical theory
ion flux
NBI counter injection
orbit loss
fast ion loss
bipolar part of Anomalous loss

Fig.11

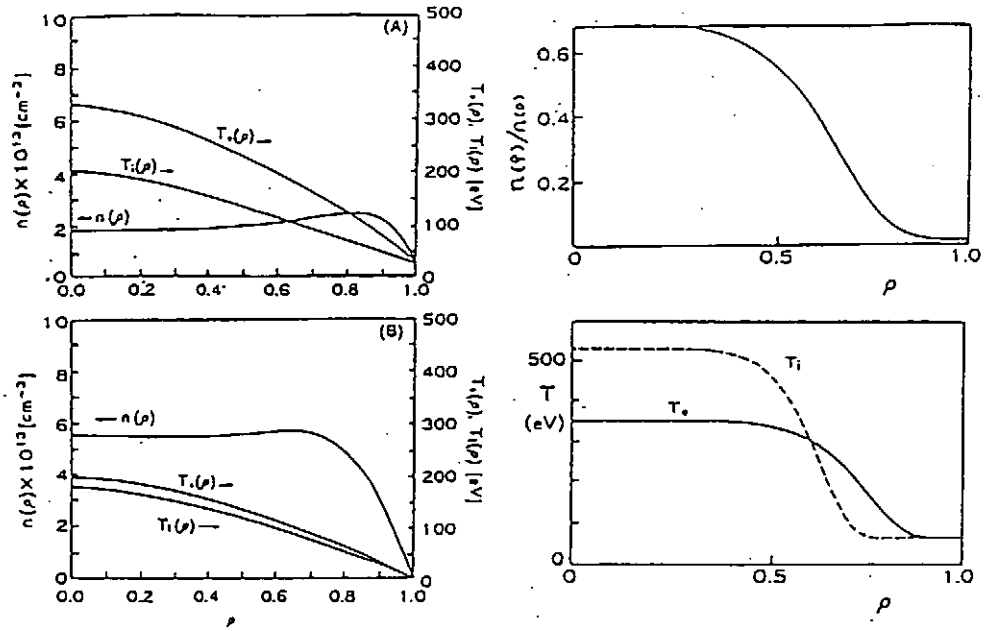

Fig.12

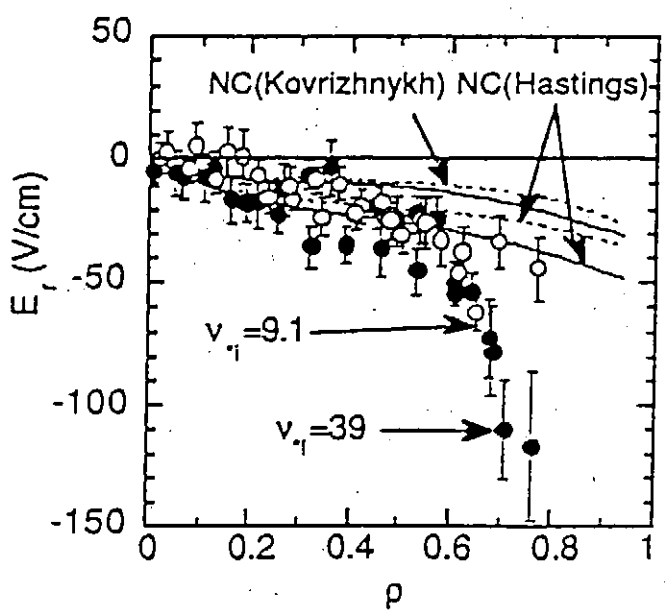

Fig.13

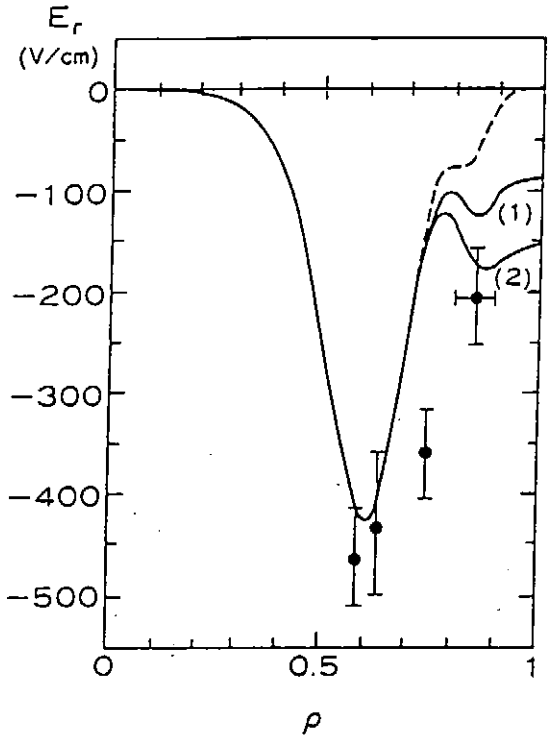
E_r
(V/cm)
0
−100
−200
−300
−400
−500
0
0.5
1
ρ
(1)
(2)

Fig.14

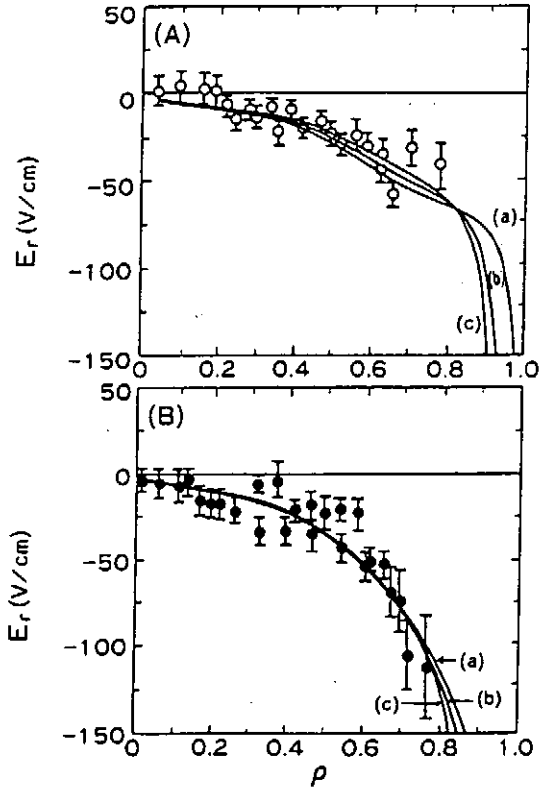
50
0
−50
−100
−150
E_r (V/cm)
(A)
(a)
(b)
(c)
0
0.2
0.4
0.6
0.8
1.0
(B)
ρ

Fig.15

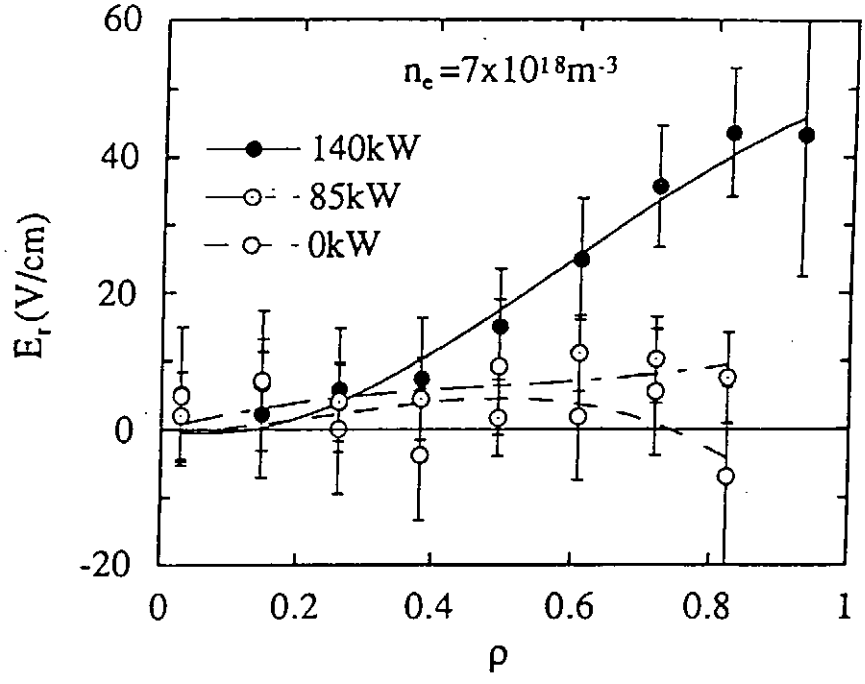
60
40
20
0
-20
E_r (V/cm)
n_e =7x10^{18}m^{-3}
140kW
85kW
0kW
0
0.2
0.4
0.6
0.8
1
ρ

Fig.16

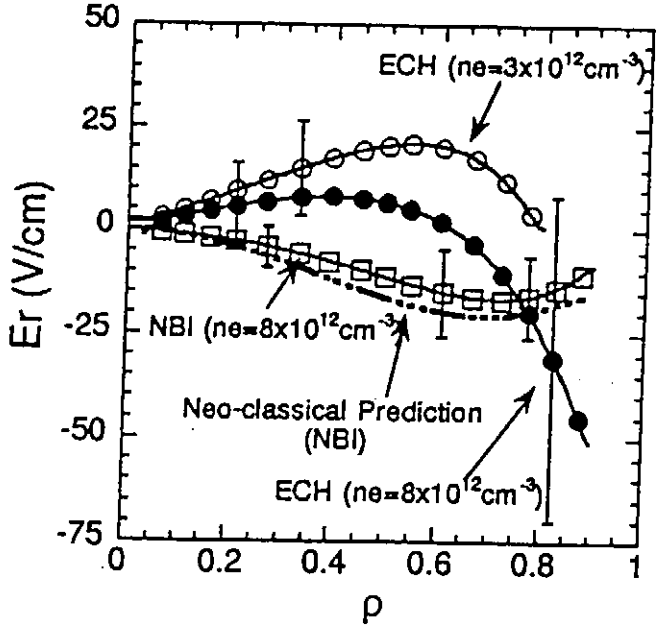
50
25
0
-25
-50
-75
Er (V/cm)
ECH (ne=3x10^{12}cm^{-3})
NBI (ne=8x10^{12}cm^{-3})
Neo-classical Prediction
(NBI)
ECH (ne=8x10^{12}cm^{-3})
0
0.2
0.4
0.6
0.8
1
ρ

Fig.17

Publication List of NIFS-PROC Series

NIFS-PROC-1 "*U.S.-Japan on Comparison of Theoretical and Experimental Transport in Toroidal Systems Oct. 23-27, 1989*", Mar. 1990

NIFS-PROC-2 "*Structures in Confined Plasmas –Proceedings of Workshop of US-Japan Joint Institute for Fusion Theory Program–* "; Mar. 1990

NIFS-PROC-3 "*Proceedings of the First International Toki Conference on Plasma Physics and Controlled Nuclear Fusion –Next Generation Experiments in Helical Systems– Dec. 4-7, 1989*" Mar. 1990

NIFS-PROC-4 "*Plasma Spectroscopy and Atomic Processes –Proceedings of the Workshop at Data & Planning Center in NIFS–*"; Sep. 1990

NIFS-PROC-5 "*Symposium on Development of Intensed Pulsed Particle Beams and Its Applications February 20 1990*"; Oct. 1990

NIFS-PROC-6 "*Proceedings of the Second International TOKI Conference on Plasma Physics and Controlled Nuclear Fusion , Nonlinear Phenomena in Fusion Plasmas -Theory and Computer Simulation-*"; Apr. 1991

NIFS-PROC-7 "*Proceedings of Workshop on Emissions from Heavy Current Carrying High Density Plasma and Diagnostics*"; May 1991

NIFS-PROC-8 "*Symposium on Development and Applications of Intense Pulsed Particle Beams, December 6 - 7, 1990*"; June 1991

NIFS-PROC-9 "*X-ray Radiation from Hot Dense Plasmas and Atomic Processes*"; Oct. 1991

NIFS-PROC-10 "*U.S.-Japan Workshop on "RF Heating and Current Drive in Confinement Systems Tokamaks" Nov. 18-21, 1991*, Jan. 1992

NIFS-PROC-11 "*Plasma-Based and Novel Accelerators (Proceedings of Workshop on Plasma-Based and Novel Accelerators) Nagoya, Japan, Dec. 1991*"; May 1992

NIFS-PROC-12 "*Proceedings of Japan-U.S. Workshop P-196 on High Heat Flux Components and Plasma Surface Interactions for Next Devices*"; Mar. 1993

NIFS-PROC-13 『NIFS シンポジウム
「核燃焼プラズマの研究を考える－現状と今後の取り組み方」
1992年7月15日、核融合科学研究所』
1993年7月

NIFS Symposium
"Toward the Research of Fusion Burning Plasmas -Present Status and Future strategy-", 1992 July 15, National Institute for Fusion Science"; July 1993 (in Japanese)

NIFS-PROC-14 "*Physics and Application of High Density Z-pinches*", July 1993

NIFS-PROC-15 岡本正雄、講義「プラズマ物理の基礎」
平成5年度 総合大学院大学
1994年2月
M. Okamoto,
"Lecture Note on the Bases of Plasma Pysics"
Graduate University for Advanced Studies
Feb. 1994 (in Japanese)

NIFS-PROC-16 代表者 河合良信
平成5年度 核融合科学研究所共同研究
研究会報告書
「プラズマ中のカオス現象」
"Interdisciplinary Graduate School of Engineering Sciences"
Report of the meeting on Chaotic Phenomena in Plasma
Apr. 1994 (in Japanese)

NIFS-PROC-17 平成5年度 NIFS シンポジウム報告書
「核融合炉開発研究のアセスメント」
平成5年11月29日-30日 於 核融合科学研究所
"Assessment of Fusion Reactor Development"
Proceedings of NIFS Symposium held on November 29-30, 1993 at National Insitute for Fusion Science" Apr. 1994
(in Japanese)

NIFS-PROC-18 *"Physics of High Energy Density Plasmas Produced by Pulsed Power"* June 1994

NIFS-PROC-19 K. Morita, N. Noda (Ed.),
"*Proceedings of 2nd International Workshop on Tritium Effects in Plasma Facing Components at Nagoya University, Symposion Hall, May 19-20, 1994*", Aug. 1994

NIFS-PROC-20 研究代表者 阿部 勝憲 (東北大学・工学部)
所内世話人 野田信明
平成6年度 核融合科学研究所共同研究 [研究会]
「金属系高熱流束材料の開発と評価」成果報告書
K. Abe and N. Noda (Eds.),
"Research and Development of Metallic Materials for Plasma Facing and High Heat Flux Components" Nov. 1994
(in Japanese)

NIFS-PROC-21 世話人:森田 健治(名大工学部)、金子 敏明(岡山理科大学理学部)
「境界プラズマと壁との相互作用に関する基礎過程の研究」

研究会報告
K. Morita (Nagoya Univ.), T. Kaneko (Okayama Univ. Science)(Eds.)
"*NIFS Joint Meeting "Plasma-Divertor Interactions" and "Fundamentals of Boundary Plasma-Wall Interactions" January 6-7, 1995 National Institute for Fusion Science*"
Mar. 1995 (in Japanese)

NIFS-PROC-22
代表者　河合　良信
プラズマ中のカオス現象
Y. Kawai,
"*Report of the Meeting on Chaotic Phenomena in Plasma,* 1994"
Apr. 1995 (in Japanese)

NIFS-PROC-23
K. Yatsui (Ed.),
"*New Applications of Pulsed, High-Energy Density Plasmas*";
June 1995

NIFS-PROC-24
T. Kuroda and M. Sasao (Eds.),
"*Proceedings of the Symposium on Negative Ion Sources and Their Applications, NIFS, Dec. 26-27, 1994*", Aug. 1995

NIFS-PROC-25
岡本　正雄
新古典輸送概論（講義録）
M. Okamoto,
"*An Introduction to the Neoclassical Transport Theory" (Lecture note)*, Nov. 1995 (in Japanese)

NIFS-PROC-26
Shozo Ishii (Ed.),
"*Physics, Diagnostics, and Application of Pulsed High Energy Density Plasma as an Extreme State*"; May 1996

NIFS-PROC-27
代表者　河合　良信
プラズマ中のカオスとその周辺非線形現象
Y. Kawai ,
"*Report of the Meeting on Chaotic Phenomena in Plasmas and Beyond, 1995*", Sep. 1996 (in Japanese)

NIFS-PROC-28
T. Mito (Ed.),
"*Proceedings of the Symposium on Cryogenic Systems for Large Scale Superconducting Applications*", Sep. 1996

NIFS-PROC-29
岡本　正雄
講義「核融合プラズマ物理の基礎 - I」
平成８年度　総合研究大学院大学　数物科学研究科　核融合科学専攻
1996年 10月
M. Okamoto
"*Lecture Note on the Fundamentals of Fusion Plasma Physics - I*"
Graduate University for Advanced Studies; Oct. 1996 (in Japanese)

NIFS-PROC-30

研究代表者　栗下　裕明（東北大学金属材料研究所）
所内世話人　加藤　雄大
平成８年度核融合科学研究所共同研究
「被損傷材料の微小体積強度評価法の高度化」研究会
1996年 10月　9日　於：核融合科学研究所

H. Kurishita and Y. Katoh (Eds.)

NIFS Workshop on Application of Micro-Indentation Technique to Evaluation of Mechanical Properties of Fusion Materials, Oct. 9, 1996, NIFS
Nov. 1996 (in Japanese)

NIFS-PROC-31

岡本　正雄
講義「核融合プラズマ物理の基礎 - II」
平成８年度　総合研究大学院大学　数物科学研究科　核融合科学専攻
1997年 4月
M. Okamoto
"*Lecture Note on the Fundamentals of Fusion Plasma Physics - II*"
Graduate University for Advanced Studies; Apr. 1997 (in Japanese)

NIFS-PROC-32

代表者　河合　良信
平成8年度　核融合科学研究所共同研究
研究会報告「プラズマ中のカオスとその周辺非線形現象」

Y. Kawai (Ed)

Report of the Meeting on Chaotic Phenomena in Plasmas and Beyond, 1996; Apr. 1997 (mainly in Japanese)

NIFS-PROC-33

H. Sanuki,
Studies on Wave Analysis and Electric Field in Plasmas; July 1997